Development of Pial Collaterals by Extension of Pre-existing Artery Tips

Suraj Kumar, Niloufer Shanavas, Swarnadip Ghosh, Vinayak Sivaramakrishnan, Manish Dwari, Soumyashree Das[#]

National Centre for Biological Sciences, Tata Institute of Fundamental Research, Bengaluru, KA 560065, India

[#] Corresponding author (soumyashree@ncbs.res.in)

Key Words

Pial Collateral Artery, Artery Endothelial Cell, Vascular Endothelial Growth Factor Receptor-2, Intra-vital Imaging, Genetic Lineage Tracing

SUMMARY

Pial collaterals provide protection from ischemic damage and improve prognosis of stroke patients. The origin or precise sequence of events underlying pial collateral development is unclear and has prevented clinicians from adapting new vascularization and regeneration therapies. We use genetic lineage tracing and intra-vital imaging of mouse brains at cellular resolution to show that during embryogenesis, pial collateral arteries develop from extension and anastomoses of pre-existing artery tips in a VegfR2 dependent manner. Our data demonstrate that an arterial receptor, Cxcr4, earlier shown to drive artery cell migration and coronary collateral development, is dispensable for formation and maintenance of pial collateral arteries. Our study reveals that collateral arteries of the brain are built by a unique mechanism, distinct from that of the heart.

INTRODUCTION

Pial (leptomeningeal) collateral arteries are an extensive network of inter-artery anastomoses found in the pial layer of the brain. In humans, the extent of pial collateral circulation is a predictor for stroke outcome.[1,2] Stroke occurs when blood supply is obstructed to a part of the brain and is one of the leading causes of morbidity worldwide (World Health Organization).[3] Pial collaterals serve as an alternate route of blood flow and alleviate the symptoms of ischemic stroke by bypassing vascular occlusions. Thus, understanding mechanisms which drive the origin and remodelling of pial collateral arteries is of immense clinical relevance.

Results from preclinical studies indicate wide-spread variation in the pial collateral artery network among individuals and organs.[4] These variations are a result of differential expression and function of proteins associated with Vascular endothelial growth factor (Vegf) signalling axis.[5–7] Different mouse strains demonstrate differential Vegfa expression level which corelate with their pial collateral density.[8] Similarly, global overexpression of Vegf ligand increases number of native pial collaterals and improve collateral perfusion post-injury.[5,6] The receptor mediating function of Vegf ligand during the formation of pial collaterals is Vegf receptor-2 (VegfR2).[6] A global knockdown of Vegf or VegfR2 during embryogenesis and in a time-frame when pial collaterals are expected to form, results in reduction in their number and diameter.[6] Thus, Vegf is a key driver of pial collateral formation and a critical factor which regulates variation in extent of pial vascular network in mice.

The vital role of Vegf in murine pial collateral development was discovered almost a decade ago.[5,6] However, it is still unclear how the various molecular players of Vegf pathway orchestrate the formation or remodelling of pial collateral network. In

mice, it is hypothesized that an *arteriole-specific sprouting angiogenesis like* process leads to the formation of the foremost pial collaterals.[6] However, molecular evidence supporting the identity of these sprouting cells (if arteries or capillaries) is missing. Additionally, the cellular origin or fate of these sprouts is unknown. Finally, the possibility of cooperation from other vascular processes, such as arterialization, arteriogenesis or artery-reassembly, in building pial collaterals, needs to be thoroughly investigated.

In this study, we use genetic lineage tracing in conjunction with live imaging of pial vasculature of transgenic mouse embryos and adults to understand mechanisms by which Vegf regulates pial collateral development and maintenance. Our data indicate that the cellular source of pial collateral arteries is primarily pre-existing artery endothelial cells (ECs) which build the first network of pial collaterals at embryonic day (e) 15.5 via VegfR2-dependent artery tip extension. While arterial VegfR2 was essential for formation of pial collaterals *de novo*, it was dispensable for its maintenance through adulthood. Arterial Cxcr4 (C-X-C chemokine receptor type-4), which is critical for coronary artery formation in mice[9] was dispensable during pial collateral formation and its maintenance. Together, our data indicate that artery endothelial cells build collateral arteries by adapting distinct vascular mechanisms in heart and brain.

RESULTS

Pial collateral arteries form during embryogenesis

We developed a whole brain imaging technique to reliably visualize all pial arteries (Figure **S1A**, **B**). Due to lack of unique markers, accurately identifying pial collateral arteries is exclusively dependent on their location. Pial collateral arteries

are artery segments which interconnect the ends of cerebral arteries and can be seen in the watershed region (Figure **S1B**). To acquire this spatial information, it was imperative to image the entire pial network. Our technique allowed us to precisely identify pial collateral arteries. We specifically focused on collateral arteries which connected and received blood flow from Anterior Cerebral Artery (ACA) and Middle Cerebral Artery (MCA) as the coverage of this arterial network is most extensive.

We first investigated the developmental stage when pial collaterals first appeared. Mouse brains were harvested at different developmental time points and whole brain immunostaining was performed for Connexin-40 (Cx40) protein, a known marker for mature artery endothelial cell. Analyses of pial arterial network in both hemispheres revealed the appearance of MCA at embryonic day e12.5 followed by ACA at e13.5 (Figure **S1C** and **S2**). At e14.5, both cerebral arteries were present with no arterial connections between them. Subsequently, the first arterial anastomoses appeared at e15.5 which then remodelled to expand in number through birth/postnatal day (P)0 (Figure **S1C** and **S2A-F**). This method confirmed that both MCA and ACA are present at e14.5 (Figure **S2G**) and the foremost pial collaterals appear at e15.5 (Figure **S2H**).

To confirm the above results, we next used a knock-in mouse line (*Cx40*$^{eGFP/+}$) where eGFP expression was driven by *Cx40* promoter activity. Brains from different developmental stages confirmed our findings from Cx40 immunostaining. MCA appeared at e12.5, ACA appeared at e14.5 and collateral arteries between MCA and ACA appear at e15.5 (Figure **S3A-F** and **S1C**). eGFP^{+} cerebral arteries (MCA and ACA) were formed by e14.5 (Figure **S3G**) and the first eGFP^{+} collateral artery between MCA and ACA appeared at e15.5 (Figure **S3H**). Thus, using two independent methods— Cx40 immunostaining and detecting its reporter activity, we

97 demonstrate that mouse pial collateral arteries form during development, and appear
98 precisely at e15.5 (Figure **S1C**).

99 **Intravital imaging reveals arterial origin of pial collaterals by artery tip**
100 **extension along microvascular tracks**

101 Despite several hypotheses, there is lack of compelling data in support of
102 vascular mechanisms which drive pial collateral development. Pial collaterals appear
103 at late embryonic stages. At this developmental stage rapid vascular changes make
104 it difficult to distinguish collateral-specific events from overall vascular growth, thus
105 making it challenging to draw information from fixed brain samples. Additionally, late
106 embryonic stages cannot be cultured *ex vivo* due to extremely demanding metabolic
107 and physiological needs. Thus, we custom-developed an imaging paradigm to
108 perform intra-vital imaging of pial layer at late embryonic stages (e16-e17) (Figure
109 **1A**), a developmental stage where the brain is actively building pial collaterals.
110 Briefly, embryos of the desired developmental time points were dissected out (with
111 their intact yolk sac) from the anesthetized pregnant mice while still connected to the
112 mother via their umbilical cord. Embryos were maintained at 37˚C and immobilized at
113 appropriate orientation to aid imaging. The embryos were subjected to stereoscopic
114 or confocal imaging for several hours. This imaging set up allowed visualization of
115 the entire hemisphere– MCA, ACA, and connected collateral arteries (Figure **1B**).

116 Pial collaterals appear only after the primary branches of MCA and ACA have
117 developed (Figure **S1C**). We hypothesized that the branches of these cerebral
118 arteries contribute towards formation of pial collaterals. To test this hypothesis,
119 *Cx40CreER; Rosa26^{TdTomato}*; *Tie2:: eGFP::Claudin5* mice were used to label artery
120 ECs with TdTomato and all endothelial cells with eGFP. To activate TdTomato,

121 Tamoxifen was administered at e13.5, when both MCA and ACA are present and
122 would be labelled in 2 days, [9,10] by e15.5. Imaging of endothelial cells derived from
123 arteries was performed at e16-e17. This experimental strategy allowed visualization
124 of cellular dynamics specific to artery cells derived from pre-existing arteries (Figure
125 **1C**) and excluded the possibility of capturing other vascular processes.

126 We performed intra-vital time-lapse imaging of pial arteries and investigated if
127 pial collaterals originate from pre-existing artery endothelial cells. We focused on the
128 watershed region: an initial artery-free region which spans the distal ends of both
129 arterial trees (MCA and ACA) and is later occupied by pial collaterals (Figure **S1C**
130 and **1D-F**). Stereoscopic images of e16.5 brains revealed that branches from MCA
131 and ACA extend (arrowheads, Figure **1E**) and anastomose to build collaterals in the
132 pial watershed (brackets, Figure **1E**). Additionally, TdTomato expression in artery
133 tips (orange arrow, Figure **1E**) and collaterals (green arrow, Figure **1E**) increased
134 over time. These changes were executed within a short span of 80 minutes, and
135 could not have been captured in fixed brain samples.

136 We next investigated artery cell dynamics associated with the growth fronts of
137 the two cerebral arteries (Figure **1F**, **G**). At e16.5, the distal branches of the
138 developing MCA extended and anastomosed to build an artery network *de novo*
139 (arrowheads, Figure **1G**). This is the first evidence demonstrating that pre-existing
140 cerebral artery tips build pial collaterals. We then performed intra-vital time-lapse
141 confocal imaging of brains at e16, a stage prior to when we observed collateral
142 artery networks being built de novo (Figure **1E**, **G**). Confocal imaging at e16 provided
143 the necessary cellular resolution to quantitatively assess artery-tip extensions from
144 MCA and ACA branches (Figure **1H-J**). As expected, we clearly observed artery tip
145 extension of MCA branch (Figure **1H**, **I**) within an hour. Additionally, we noted

146 several artery-specific movements within the pial layer. This included the
147 appearance of single artery endothelial cells (arrows, Figure **S4A**, **B**), movement of
148 these single artery cells towards an artery (Figure **1J**, Figure **S4C**), and emergence
149 of arterial sprouts (arrowheads, Figure **S4A**, **B**). Most interestingly, all artery cell
150 movements were observed along microvascular tracks which appeared structurally
151 more organized/tubular than the surrounding capillaries (arrowheads, Figure **1K** and
152 Figure **S4A**, **D**). These "microvascular tracks" were distinct from the surrounding
153 capillary plexus in that they formed direct connections between two arteries but were
154 not entirely populated by TdTomato^{+} artery derived endothelial cells (Figure **1K** and
155 Figure **S4A**, **D**). Together, for the first time, we provide direct evidence for the
156 vascular origin of pial collaterals— pre-existing MCA/ACA artery tips grow on distinct
157 microvascular paths and connect with each other to build pial collaterals *de novo*
158 (Figure **1L**).

159 **Artery ECs are the major cellular contributors of pial collaterals during**
160 **embryogenesis**

161 We next assessed the vascular-lineage composition of pial collaterals at a
162 later stage when the collateral artery network has fully formed. This would allow us
163 to: 1) determine if the artery cell contribution to nascent pial collaterals observed at
164 e16.5 (Figure **1E**) persisted in later stages and 2) check contribution from
165 microvascular lineage which is evident in newly formed collaterals in heart[9,11] and
166 skeletal muscle.[12] Genetic lineage tracing with *Cx40CreER Rosa26^{TdTomato}* and
167 *ApjCreER Rosa26^{TdTomato}* mice were performed where TdTomato expression could
168 be conditionally induced, with Tamoxifen, specifically in artery ECs or capillaries
169 respectively. Tamoxifen was administered to timed pregnant mice at e14.5 when
170 both MCA and ACA arteries are present (Figure **2A**, **S2G**, **S3G**). Embryos were

171 analysed at e18.5 or P0 when the pial collateral artery network has completely
172 formed (Figure **2A**, **S2H**, **S3H**). Whole embryonic brains were immunostained for
173 Cx40 and segments of collateral arteries between MCA and ACA were analysed for
174 lineage contribution (Figure **2B-J**).

175 We assessed the extent of lineage contribution from artery or capillary ECs
176 towards pial collaterals. As expected, all pre-existing artery ECs were labelled and
177 traced in *Cx40CreER; Rosa26*^{TdTomato} embryos (Figure **2C**, **D**, **G**, **I**). Whole brain
178 imaging of the embryo (Figure **2C**) allowed identification of pial collateral arteries
179 present between MCA and ACA in the watershed (Figure **2D**). Individual collateral
180 segments as identified by Cx40 immunostaining were analysed for presence of
181 TdTomato^{+} artery ECs (Figure **2D**, **G**, **I**). This analysis revealed that 77% of the
182 Cx40^{+} collateral area to be TdTomato^{+} (Figure **2B**). In contrast to this data, a similar
183 analysis in an independent experiment with *ApjCreER; Rosa26*^{TdTomato} mice (Figure
184 **2E**, **F**, **H**, **J**) showed only 31.6% of the collateral area to be TdTomato^{+}, i.e. traced
185 from capillaries (Figure **2B**). Thus, artery ECs are the major contributors of pial
186 collateral arteries during development.

187

188 **Arterial VegfR2 mediates artery tip extension and is essential for pial collateral**
189 **artery development**

190 We analysed similarities, if any, in the molecular programs used by artery
191 endothelial cells during collateral development in the heart and brain. Post-injury,
192 neonatal coronary artery ECs undergo extensive migration and proliferation to build
193 new coronary collateral arteries in the watershed. The processes of artery cell
194 migration and proliferation are heavily dependent on Cxcr4[9] and VegfR2[13]
195 respectively. To assess the functions of Cxcr4 and VegfR2 in pial collateral

196 development, we deleted the respective genes at e14.5 and assessed the extent of
197 pial collateral network at e18.5/P0 by whole brain imaging (Figure **3A**). Surprisingly,
198 deletion of arterial *Cxcr4* did not affect the pial collateral network at e18.5 (Figure **3B**,
199 control=8, artery specific knockout for *Cxcr4*=13) or in adulthood (Figure **S5**, N=5 per
200 genotype). This data suggests that a Cxcr4-independent vascular mechanism
201 facilitates pial collateral development and its maintenance.

202 We next assessed if pial collateral artery development is dependent on
203 arterial VegfR2. Whole brain imaging of control and *VegfR2* artery specific knockout
204 embryos showed differences in collateral connectivity in the watershed, and required
205 systematic quantification (Figure **3C-F**). The extensive connectivity of pial arteries
206 across the hemisphere (including watershed) provide several possible collateral
207 paths for the blood to flow. These artery-artery connections are innumerable. We
208 developed a method that allowed us to compare the pial artery coverage between
209 the control and *VegfR2* artery EC specific knockout brains quantitatively (Figure **3C**).
210 Intensity line-profiles were generated across the width of the hemisphere (Figure **3C**
211 **i**, **ii**). The identified peaks per line-profile was plotted across the width of the
212 hemisphere (Figure **3C iii**). The data was fit to a gaussian function and the fitted
213 curves were used as representative of the arterial coverage per hemisphere in each
214 mouse (Figure **3C iv**). The average of the fitted curve represented one mouse brain
215 (grey curve, Figure **3C iv**). This curve represented the artery coverage per
216 hemisphere. Quantification of pial artery coverage showed significantly different
217 distributions between control and *VegfR2* knockout brains (KS test, D value=0.569, p
218 value=2.2066×10^{-141}) (Figure **3E)**. Peak arterial coverage was observed at the
219 centre of the hemisphere and watershed was defined as a region ± 500μm from the
220 centre (Figure **3E**). The loss of arterial coverage in the watershed was evident in the

221 knockout (Figure **3E**) and was quantified as area under the curve (Figure **3E**, **F**).
222 This area under the curve represented the extent of collateral artery network in the
223 watershed and was significantly lower in brains without arterial *VegfR2* (Figure **3F**,
224 unpaired t-test, p value= 0.0001). Thus, *VegfR2*-depleted arteries were unable to
225 synthesize pial collaterals during embryogenesis.

226 We next investigated the possible mechanisms by which arterial VegfR2
227 facilitated pial collateral formation. *VegfR2* was deleted from artery ECs at e14.5,
228 and analyses of pial collateral network was performed at e16.5 (Figure **3G**), a
229 timepoint when collaterals are beginning to form via artery tip extensions (Figure **1D-**
230 **G**)**.** Quantification showed fewer TdTomato^{+} collateral arteries (i.e. TdTomato
231 continuous or Td^{con}) without arterial *VegfR2* (Figure **3H**), indicating that initiation of
232 collateral development at an earlier timepoint, e16.5, also depends on arterial
233 *VegfR2*. This VegfR2-dependent collateral phenotype (Figure **3H**) was independent
234 of artery cell proliferation which was minimal at this stage, for both control and
235 *VegfR2*-deleted brains (data not shown). Close analyses of collaterals in control
236 brains showed that TdTomato^{+} artery cells occupied a major length of microvascular
237 tracks connecting branches of MCA and ACA (Figure **3I**). This observation was in
238 contrast to *VegfR2*-depleted brains where TdTomato^{+} artery cells sparsely populated
239 the microvascular tracks (Figure **3J**). Thus, arterial VegfR2 regulates pial collateral
240 formation by promoting artery growth along microvascular tracks.

241 We investigated if endothelial cells of capillary lineage populate pial collaterals
242 via Dach1; a transcriptional factor that drives arterialization of capillaries into
243 coronary arteries during cardiac development in mice.[14] As observed in developing
244 mouse hearts,[14,15] expression of Dach1 was higher in capillaries as compared to
245 arteries (Figure **S6A**). *Dach1* was deleted from capillaries at e14.5 and the extent of

246 pial collateral network was assessed at e18.5 (Figure **S6B**). Interestingly, no
247 significant difference was observed in the number of Cx40^{+} collaterals in the *Dach1*
248 capillary-EC specific knockout brains (Figure **S6C**). This suggests that the vascular
249 mechanism which leads capillaries to populate pial collaterals is independent of
250 Dach1 activity.

251 **Pial collaterals do not remodel in adulthood**

252 We next investigated the cellular dynamics associated with fully formed and
253 mature pial collateral arteries between MCA and ACA in adult mice. For this, we
254 utilized an extensive longitudinal in vivo imaging paradigm that allowed us to get
255 single cell resolution of vascular structures. 3-5 months old *Cx40CreER;*
256 *Rosa26^{TdTomato};Tie2::eGFP::Claudin5* mice underwent craniotomy and an optical
257 window of 4mm was implanted on one of the hemispheres between the cranial
258 landmarks—bregma and lambda (Figure **4A**, **B**). In these transgenic mice, pre-
259 existing pial arteries were labelled with TdTomato upon Tamoxifen administration
260 (Figure **4C**), and constitutively expressing GFP marked all endothelial cells. 5
261 consecutive doses of Tamoxifen resulted in 95.4% and 86.8% recombination in
262 proximal and distal arteries respectively, but a lower 65.3% recombination in the pial
263 collateral regions (Figure **4D**). A lower recombination efficiency in the pial collateral
264 arteries resulted in a patchy reporter pattern comprising of a mixture of TdTomato^{+}
265 and TdTomato^{-} cells (Figure **4D**). Like in developmental stages (Figure **2B**), artery
266 ECs populate adult pial collaterals to a greater extent as compared to other vascular
267 lineages. This ultimately allowed us to most accurately track the position of individual
268 cells within a given collateral artery.

269 An optical window allows longitudinal imaging. Imaging the collateral zone
270 (watershed between MCA and ACA) for a month (Figure **4E**), resulted in high quality
271 images with single cell resolution (Figure **4E-H**). Morphology of the pial vessels
272 alongside reporter activity in endothelial cells were instrumental in identifying pial
273 arteries, veins and capillaries (Figure **4E**, **I**). High resolution images of artery
274 endothelial cells (both TdTomato^{+} GFP^{+} and TdTomato^{-} GFP^{+}) within a collateral
275 artery segment across many collaterals and optical windows were analysed (Figure
276 **4J**, **K**). Data showed that artery endothelial cells do not remodel or reposition
277 themselves within a given collateral artery segment (Figure **4J-M**). Cellular matrices
278 representative of the relative position of collateral artery cells suggested that under
279 physiological conditions, every artery cell within a mature/ adult pial collateral
280 maintains its contact with the same neighbouring cells (Figure **4L**, **M**). Thus, for the
281 first time our data, with cellular resolution, demonstrates the static nature of artery
282 endothelial cells during homeostasis.

283 **Arterial VegfR2 is dispensable for pial collateral maintenance**

284 We next asked if arterial VegfR2 is necessary for the maintenance of adult
285 pial collaterals using adult mice deficient in arterial *VegfR2*. Using the same in vivo
286 imaging paradigm mentioned above, pial collateral segments in artery endothelial
287 cell specific *VegfR2* knockout mice were imaged at cellular resolution and followed
288 for a month with imaging time-points separated by 2 weeks (Figure **5A**). Longitudinal
289 imaging through an optical window (Figure **5B**) yielded a map of vascular network
290 which could be followed for months (Figure **5C**, **D**). Of note, our qualitative
291 observation suggests that *VegfR2* depleted pial collaterals had smaller diameters.
292 High magnification images of watershed between MCA and ACA (Figure **5E-G**)
293 allowed us to analyse individual *VegfR2*$^{-/-}$ artery endothelial cells (TdTomato^{+})

294 residing on adult collateral arteries (Figure **5H-J**). Long term imaging of the same
295 collateral regions across many collaterals and mice showed no significant changes in
296 cellular positions relative to the neighbouring cells (Figure **5K-M** and Figure **S7**).
297 Thus, arterial VegfR2 is dispensable for maintenance of mature pial collateral
298 arteries. Together, in this study, we highlight the essential role of arterial VegfR2 in
299 promoting artery-tip extension and pial collateral development during embryogenesis
300 (Figure **5N**); a function dispensable in adulthood.

301 **DISCUSSION**

302 In the present study, we investigate artery cell dynamics during collateral artery
303 formation and maintenance in mouse brain. Firstly, using an artery-specific
304 molecular marker, we dissect out where and when pial collaterals appear during
305 embryogenesis. Secondly, we develop a live imaging method of mouse embryos to
306 provide conclusive evidence that pre-existing arteries grow and connect to build pial
307 collaterals *de novo*. Thirdly, by combining mouse genetics with whole brain confocal
308 imaging at cellular resolution, we show an angiogenic vascular receptor VegfR2,
309 facilitates artery-tip extension on microvessels and aids origin of pial collaterals.
310 Finally, we show that Cxcr4, a receptor essential for Artery Reassembly and
311 formation of coronary collateral arteries *de novo*, was dispensable for development
312 of pial collaterals. Thus, two fundamentally distinct mechanisms contribute to the
313 origin of coronary and pial collaterals.

314 **Organ-specific mechanisms build collaterals**

315 For the first time, we provide direct proof that a vascular mechanism driven
316 specifically by artery endothelial cells leads to the origin of pial collaterals. Like in the
317 heart, this artery specific process is regulated by arterial VegfR2, but is distinct from

318 Artery Reassembly where pre-existing artery cells dissociate from resident
319 coronaries, migrate, de-differentiate/proliferate and coalesce to build coronary
320 collaterals.[9,13] Unlike heart, pial artery endothelial cells provide minimal contribution
321 via proliferation. Instead, developing pial arteries extend along microvascular tracks
322 and connect with other artery tips to build new collateral artery paths. These
323 endothelial cells which migrate or elongate along the microvasculature could arise
324 from proximal parts of the cerebral arteries. Additionally, arterial Cxcr4 had no impact
325 on pial collateral formation or its maintenance. This is in contrast to coronary
326 collateral formation where arterial Cxcr4 drives artery cell migration during Artery
327 Reassembly. The need for functional collaterals is most during an artery occlusion,
328 and can significantly impact tissue function. The similarities and differences between
329 the origin of coronary and pial collaterals could be driven by the metabolic needs of
330 the tissue. While cardiomyocytes can survive hypoxia for few hours, neurons are
331 more susceptible to low levels of oxygen.[16,17] The differences in sensitivity to hypoxia
332 could be the reason for formation of pial collaterals during embryogenesis while
333 coronary collaterals form only upon arterial occlusion. Furthermore, collateral arteries
334 found in skeletal muscle,[11,18] intestine,[19] and hind limb[20] can undergo
335 arteriogenesis.[21] Identifying collateral-building vascular mechanisms across organs
336 could reveal clinically relevant information and open avenues for therapeutics.

337 **Old arteries build new arteries**

338 We demonstrate the formation of collateral arteries from pre-existing arterial
339 lineage as observed[9,10,13,22] or proposed[6] earlier. While this manuscript was in
340 progress, Perovic et al reported that two separate vascular lineages populate pial
341 collaterals.[10] We also observed that well-formed pial collaterals are majorly

342 populated by artery cells, and minimally by capillaries. Intra-vital imaging of
343 embryonic brains reveal that pre-existing artery cells extend along defined
344 microvascular paths to connect and build pial collaterals. These artery specific
345 events are executed within hours, are difficult to capture using static images and can
346 be observed only by live imaging. We cannot exclude the contribution of other artery-
347 driven mechanisms, such as migration of single artery cells from proximal segments
348 of cerebral arteries and their incorporation into pre-existing artery tips leading to
349 further artery elongation. The capillary contribution towards pial collaterals via
350 arterialization is less likely as deletion of *Dach1*, a regulator of arterialization,[14,23] had
351 minimal effect on pial collateral network during embryogenesis. We propose that as
352 artery tips extend and get connected in the watershed, microvascular cells are
353 "trapped" within pial collaterals. This could generate a mixed lineage distribution[10]
354 within pial collaterals—both in embryos and adults.

355 We also observed artery cells migrating towards pre-existing arteries;
356 coalescence of these single cells with arteries could lead to arterial growth as
357 observed during Artery Reassembly in heart. Thus, multiple mechanisms could be
358 actively building pial vasculature during embryogenesis. That being said, possible
359 contribution from endothelial progenitor cells or peri-vascular cell types (pericytes,
360 smooth muscle cells) towards pial collateral formation cannot be entirely excluded.
361 Given that collateral arteries have a unique hemodynamic niche,[24] it would be
362 interesting to investigate which molecular programs maintain or remodel pial
363 collaterals in an adult brain.

364 **Distinct mechanism for collateral maintenance**

365 During embryogenesis, pial collaterals are built *de novo*, in an artery-free
366 zone and remodel as and when blood flows through them. In contrast mature
367 collaterals remodel in response to differential blood flow pattern and oxygen
368 demands of surrounding tissue. Postnatal remodelling of pial collaterals is dependent
369 on recruitment of smooth muscle cells and exhibits tortuous morphology.[24] These
370 fundamental differences could explain the requirement for distinct molecular
371 programs for building new collaterals and maintaining old ones. This is evident in our
372 study; VegfR2 controlled pial artery network during embryogenesis but was
373 dispensable in adulthood. That being said, arterial VegfR2 may regulate other
374 aspects of vascular changes those require activation of angiogenic pathways[25] such
375 as remodelling induced by hypoxia, ischemia or aging. We did not notice any
376 remodelling events within adult pial collaterals, in presence or absence of arterial
377 Cxcr4. Together, adult pial collaterals are maintained via mechanisms independent
378 of two key angiogenic receptors in arteries—VegfR2 and Cxcr4. It will be interesting
379 to test if adult collateral maintenance is independent of signals originating from
380 arterial niche. It is possible that surrounding microvasculature plays a greater role in
381 maintenance of pial arteries and collaterals in adults. Investigating the molecular
382 identity of the microvasculature surrounding pial collaterals could reveal new
383 vascular mechanisms key to collateral maintenance.

384 **MATERIALS AND METHODS**

385 **Mouse lines**

Mouse lines	**Source/ References**
Rosa26^{TdTomato}	The Jackson Laboratory, stock number 007909
Cx40CreER	Miquerol et al. 2015[26]

ApjCreER	Chen et al. 2014[15]
VegfR2 flox	The Jackson Laboratory, stock number 018977
Cx40$^{eGFP/+}$	Miquerol et al. 2004[27]
Tie2::eGFP::Claudin5	Knowland et al. 2014[28], Lutz et al. 2017[29]
Cxcr4 flox	The Jackson Laboratory, stock number 008767
Dach1 flox	Chang et al. 2017[14]

386

387 All experiments were performed on mice with mixed strain background. All mice were
388 housed and bred at the National Centre for Biological Sciences animal facility (in
389 accordance with the Institutional Animal Ethics Committee). Tamoxifen regimes for
390 individual experiments are explained in the respective experimental sections (see
391 below). Data shown in this study is compiled from age-matched males and females
392 from several litters.

393 **Genotyping primer information**

Primer (F, forward; R, Reverse)	**Sequence (5' → 3')**
Cre F	GCATTACCGGTCGATGCAACGAGTGATGAG
Cre R	GAGTGAACGAACCTGGAAATCAGTGCG
Cre Internal positive control F	CTAGGCCACAGAATTGAAAGATCT
Cre Internal positive control R	GTAGGTGGAAATTCTATCATCC
TdTomato mutant F	CTGTTCCTGTACGGCATGG
TdTomato mutant R	GGCATTAAAGCAGCGTATCC
TdTomato wild-type F	AAGGGAGCTGCAGTGGAGTA
TdTomato wild-type R	CCGAAAATCTGTGGGAAGTC

VegfR2 flox F	CCACAGAACAACTCAGGGCTA
VegfR2 flox R	GGGAGCAAAGTCTCTGGAAA
GFP F	GCACGACTTCTTCAAGTCCGCCATGCC
GFP R	GCGGATCTTGAAGTTCACCTTGATGCC
Cxcr4 flox F	CCACCCAGGACAGTGTGACTCTAA
Cxcr4 flox R	GATGGGATTTCTGTATGAGGATTAGC
Dach1 flox F	CTCCTGAAGATGAGGAGCTCACCCC
Dach1 flox R	AACAATTCTTGTCCTTCACGTGCCC

394

395 **Visualization of pial arteries in fixed samples**

396 **Harvesting whole brains/heads from mouse embryos**

397

398 Depending on the developmental stages and size of the embryos, pial collateral
399 arteries were visualized either in whole brains (e18.5 or P0) or using whole heads
400 (e12.5- e16.5).
401 e12.5-e16.5: To perform the whole head explant at e12.5-e16.5 stages, the pregnant
402 females were euthanized as mentioned above. Small punctures were made on the
403 embryo sac with the help of microforceps. The whole embryo sac was fixed in 4%
404 Paraformaldehyde (PFA) for 2 hours with gentle shaking at 4°C. Following fixation,
405 the embryo sac was washed at 4°C with gentle shaking. This washing step was
406 performed with 1X PBS ad repeated 4 times every 15-20 mins interval. The embryos
407 were then extracted from the embryo sacs and the heads were removed with the
408 help of microforceps. Finally, specifically for e16.5, the loose skin on top of the brain
409 was removed to aid immunostaining.

410 e18.5: To perform the whole brain explant at e18.5 stage, the timed pregnant
411 females were euthanized through carbon dioxide overdose and a Y-shape incision
412 was made on the abdomen. First the embryo sac was dissected out followed by
413 careful removal of embryos from their sacs. The skull of each embryo was gently
414 removed using the microforceps. The embryonic brains were scooped out with the
415 help of a microspatula and fixed in 4% PFA at 4°C for 2.5 hours. Agitation was
416 avoided at this stage to preserve tissue integrity of embryonic brains. The fixed
417 embryonic brains are then washed with 1X PBS three times at 15 minutes intervals
418 with gentle shaking at 4°C.
419 P0: Neonatal explants at P0 were performed by euthanizing the pups through carbon
420 dioxide overdose followed by decapitation. The skull was removed using scissors
421 and microforceps. The brains were scooped out using the microspatula. The brains
422 were then fixed using 4%PFA at 4°C for 2 hrs followed by three washes with 1X PBS
423 at an interval of 15 mins.
424
425 **Whole brain/head immunostaining of mouse embryos**
426
427 e12.5-e15.5: The embryonic heads (e12.5 - e15.5) were incubated in 0.1% PBST
428 (0.1% TritonX-100 in 1X PBS) for 2.5 hours to permeabilize the tissue, followed by
429 incubation with primary antibodies overnight at 4°C with gentle shaking. Heads were
430 then washed with 1X PBS, changing the buffer every 1-2 hours for 1 day. This step
431 was followed by incubation with secondary antibodies made in 0.1% PBST. Samples
432 were then washed every 1-2 hours for 1 day with 1X PBS. Following immunostaining
433 the brains are immersed in an anti-fade mounting media (from Jackson
434 ImmunoResearch Laboratories Inc.) and imaged immediately.

435

436 e16.5: The embryonic explant at e16.5 is performed similarly. However, for
437 *Tie2::eGFP::Claudin5* genotype, whole heads were imaged within 4 hrs, prior to PFA
438 fixation to avoid loss of GFP fluorescence signal.

439

440 The embryonic and neonatal brains were incubated with primary antibody (made in
441 1X PBS) overnight, at 4°C with gentle shaking. Samples were then washed with 1X
442 PBS, changing the buffer every 1-2 hours for 1 day and incubated with Alexa Fluor
443 conjugated secondary antibodies (made in 1X PBS). Finally, samples were washed
444 every 1-2 hours for 1 day with 1X PBS and stored in mounting media or imaged
445 immediately.

446

447 Antibodies used are: Cx40 (Catalog number: Cx40-A, Alpha Diagnostics, 1:500
448 dilution), Dach1 (Catalog number: 10194-1-AP, Proteintech, 1:500 dilution), VegfR2
449 (Catalog number: AF644, R&D Systems, 1:250). All secondary antibodies were
450 procured from Invitrogen and used at a dilution of 1:500.

451

452 **Imaging whole brain/heads of mouse embryos**

453

454 The mice heads and brains were imaged using Olympus FV-3000 inverted confocal
455 microscope by placing the sample in a 2-well chamber Catalog number: 154461;
456 Nunc™ Lab-Tek™ II Chamber Slide™ System; Thermofisher Scientific. Whole
457 brains and heads were scanned using 4X and 10X air objectives, and digital images
458 of multiple stacks for each scanned area were captured. The captured images were
459 processed in ImageJ and stitched together using Adobe Photoshop software.

460

461 The embryonic heads at e16.5 was imaged using Olympus FV-3000 5L Upright
462 microscope. The pre-fixed embryonic heads were attached to a 35mm plastic petri
463 dish using agarose gel prior to imaging. The whole head imaging was performed
464 using 4X air objective and watershed images were captured with 20X water
465 dipping/immersion objective and 1.5X optical zoom with brains immersed in 1X PBS.

466

467 **Visualization of pial arteries in live mice**

468 **In vivo imaging of embryonic pial arteries**

469 Immobilization of live embryo: *Cx40CreER; Rosa26^{TdTomato}*; *Tie2::eGFP::Claudin5*
470 Pregnant dams with embryos at developmental stages between embryonic day
471 (e)15.5-e16.5 were anesthetized with a subcutaneous injection of Ketamine-Xylazine
472 (Ketamine (0.05 mg/kg); Xylazine (0.5 mg/kg)) cocktail. The dams were then placed
473 in a supine position on a regulated heating pad (TC1000, CWE) that was positioned
474 on top of a 3D-printed baseplate (as shown in Figure 1B). A small incision was
475 placed along the midline of the abdomen. With a gentle retraction of the abdominal
476 skin and wall, a single uterine horn within the abdominal cavity was isolated. The
477 uterus was surgically opened and a single embryo along with the yolk sac was
478 isolated and placed into a 35mm petri dish. The embryo still connected to the dam
479 was immobilized by submerging the bottom part with 1% agarose, as shown in figure
480 1B. The immobilized embryo is then submerged in dissection media (DMEM/F12 +
481 10% FBS, Catalog number: 21041025, Thermo Fisher Scientific), and the media is
482 maintained at 37°C using a custom-made Arduino controlled media heating and
483 circulating device.

484

485 Live embryonic imaging: The setup along with anesthetized dam was placed under
486 Macro Zoom microscope MVX10-Olympus for large scale imaging and under
487 FV3000 upright confocal Microscope-Olympus for high resolution imaging using 20X
488 water dipping objective. In Macro Zoom Microscopy, the entire observable depth was
489 scanned whilst obtaining videos of 1 minute spanning a duration of 1-2 hours in a
490 time-lapse manner. In confocal microscopy, the entire observable depth was
491 scanned with a step size of 1 micron. A total of 4 embryos were imaged under the
492 Macro zoom microscope and 5 embryos were imaged using confocal microscope.
493 Out of these embryos, the artery cell dynamics was captured in 2 brains from each
494 category.
495
496 Image processing: Image stacks obtained from Macro zoom microscopy was
497 registered using ImageJ plugin (*StackReg*) and the registered stack was de-
498 convolved using ImageJ plugin (*DeconvolutionLab2*) and finally maximum intensity
499 projection was obtained as shown in figure 1C. The image stacks obtained from the
500 confocal microscopy were processed similarly except the deconvolution step.
501
502 **In vivo imaging adult pial arteries**

503 Craniotomy: *Cx40CreER; Rosa26^{TdTomato}; Tie2::eGFP::Claudin5 and*
504 *VegfR2^{flox};Cx40CreER; Rosa26^{TdTomato};Tie2::eGFP::Claudin5* adult mice (>2
505 months) underwent craniotomy to obtain optical access to the pial layer of the brain.
506 Mice were anesthetized under 2% Isoflurane (Abbott, North Chicago, IL, USA) and
507 were placed on a stereotaxic mount (Item number 51547; Stoelting, Wood Dale, IL,
508 USA) with the skull held tightly using ear bars. The mice were kept anesthetized with
509 2% Isoflurane using a nose-cone. 5mg/kg Dexamethasone in 1X PBS was

510 administered subcutaneously and the mice kept warm using a heating pad (TC1000,
511 CWE). The eyes of the animals were covered with an eye ointment and the hair
512 above the skull removed using a hair trimmer. The surgical area was thoroughly
513 wiped clean with 70% ethanol. Sterile surgical tools are used for the surgery. A small
514 incision was made using a scalpel blade and the exposed skin was removed. The
515 connective tissue covering the skull in the exposed area was scraped off using
516 scalpel blade and Q-tips. Using a high-speed electrical drill (burr of diameter
517 ~0.25mm), a window of ~4mm diameter was carefully etched on the skull. The skull
518 within the window was eventually detached from the rest of the skull after repeated
519 drilling and carefully lifted using a pair of fine forceps (Catalog number: 11255-20,
520 Dumont #55) without damaging the dura. During the process of drilling the skull was
521 constantly irrigated with cortex buffer (Concentration; in mM: NaCl–125, KCl–5,
522 glucose–10, HEPES–10, $CaCl_2$–2 and $MgCl_2$–2. pH set to 7.35).[30] The exposed dura
523 was aspirated with cortex buffer until there is no bleeding and the window looked
524 clear. An optical plug made up of two 4 mm coverslip and one 5 mm coverslip (CS-
525 5R & CS-4R; Warner Instruments, Hamden, CT, USA) glued together (with NOA 68,
526 Norland Optical Adhesive) was placed on the exposed dura. The optical plug was
527 gently pressed using a toothpick such that the 5mm cover slip was touching the skull
528 bone and then cyano-acrylic glue was applied across the perimeter of the 5mm
529 coverslip attaching it to the skull. At this stage we had an optical window of 4mm. An
530 aluminium head bar with circular hole of 8mm was placed onto the skull aligned to
531 the previously made optical window. Next, dental cement (Catalog number 56877,
532 3M Relyx U200) was applied over the exposed skull using a sterile toothpick while
533 being careful to not get it on the optical window. Once the dental cement was
534 completely dry, the animal was placed on a warm pad in a clean recovery cage.

535 Animals undergoing craniotomy were maintained on meloxicam (2 mg/kg) and
536 enrofloxacin (5 mg/Kg body weight) for 3-4 days until full recovery. Mice were further
537 allowed to recover for at least 2 weeks post-surgery before the start of any
538 experiment. Mice with an optical window can be imaged longitudinally for 2-3 months
539 until the optical window starts to lose its clarity.
540
541 Live Adult Imaging: To perform in vivo imaging, mice were anesthetized through
542 intraperitoneal injection of Ketamine (80mg/Kg body weight) – Xylazine (5mg/Kg
543 body weight) cocktail. The eyes were covered with an eye ointment and the mice
544 were placed onto a custom-made baseplate and immobilized using the implanted
545 metal head plate to this baseplate. A heating pad (37°C) was placed under the
546 mouse to maintain the body temperature. Subsequently, the baseplate was placed
547 on a motorized XY-table of an upright confocal microscope (FV3000 upright confocal
548 Microscope-Olympus). The entire optical window was imaged using 10X air objective
549 (0.4 NA) and selected pial regions with collateral arteries were imaged with 20X
550 water immersion objective (0.5 NA). A total of N=3 adult mice per group (control and
551 *VegfR2* artery endothelial specific knockout) were imaged longitudinally for a period
552 of a month.
553
554 Image processing: The 10X image stacks obtained from the confocal microscopy of
555 the cranial window were registered using ImageJ plugin (*StackReg*) and maximum
556 intensity projection was obtained. The region of interest from the 20X image stacks
557 were cropped out slice by slice and stitched in Adobe Photoshop to avoid the
558 overlaying microvascular network in order to focus on the pial collaterals.

559 **Quantifications**

560 **Lineage contribution towards pial collaterals during embryogenesis**

561 Cx40 immunostained pial collateral segments from either *Cx40CreER;*
562 *Rosa26*^{Tdtomato} or *ApjCreER; Rosa26*^{TdTomato} brains were imaged at 10X with 2.12
563 optic zoom. Regions of interest were manually drawn to mark the collateral artery
564 segments. Lineage contribution was determined by quantifying TdTomato^{+} coverage
565 on the collateral segment. This was performed by thresholding the images with Otsu-
566 Red tool in ImageJ. The area fraction of the TdTomato^{+} area per collateral segment
567 was calculated using the Measure tool in ImageJ. Contribution of the artery and
568 capillary derived ECs in collaterals was quantified by calculating the percentage of
569 collateral area covered by TdTomato^{+} signal. 45 collateral segments (of an
570 approximate length or 600-800μm) from 7 *Cx40CreER*-lineage traced brains and 57
571 collateral segments from 8 *ApjCreER*-lineage traced brains were analysed.

572 **Number of collateral arteries per hemisphere**

573 In *Cx40CreER* TdTomato labelled brains, the collateral number was quantified based
574 on the number of continuous TdTomato^{+} vessels (Td-continuous) connecting MCA
575 and ACA. Data shown in Figure **3H** was summarized from 2 control and 3 artery-
576 specific VegfR2 knockout. Data shown in Figure **S2H** was summarized from e13.5
577 (N=3), e14.5 (N=3), e15.5 (N=2), e18.5 (N=2) and P0 (N=5) embryos and neonates.
578 Data shown in Figure **S6C** is quantified by counting number of Cx40 immunostained
579 collateral arteries between MCA and ACA, and is summarized from 4 control and 7
580 *Dach1* capillary specific knockouts. An unpaired t-test was done to test significance
581 statistically.

582 **Efficiency of Cre recombination**

583 Segments of collateral arteries, proximal arteries (PA) and distal arteries (DA) from
584 the image stacks taken with 20X objective were obtained from live adult imaging of
585 *Cx40CreER*;*Rosa26*^{TdTomato};*Tie2::eGFP::Claudin5* mice. Tdtomato^{+} and Tdtomato^{-},
586 cells were counted in each artery segment. Each segment was of an approximate
587 length of 600-800μm.The recombination efficiency was measured as ratio of
588 TdTomato^{+} cells and total number of cells in the segment. A total of 10 collateral
589 segments, 10 PA segments and 10 DA segments from 4 mice were analysed to
590 obtain the recombination efficiency of Cre. One-way ANOVA was done to test
591 significance statistically (Tukey test, p=0.0001).

592 **Pial artery coverage in whole brains and in the collateral zone**

593 The image stacks were obtained using confocal imaging of whole embryonic brains
594 with 10X objective, stitched using ImageJ plugin (stitching) and max intensity
595 projection (MIP) was obtained. The MIPs were used for further analysis wherein one
596 complete hemisphere was cropped out and aligned vertically to the major axis of its
597 own elliptical boundary. Using a custom ImageJ macro, a line of the length of the
598 major axis was scanned across the width of the image and intensity profile for every
599 pixel along the horizontal axis was generated. Total number of local maxima (peaks)
600 for each intensity profile was obtained using the built-in ImageJ macro function
601 *Array.findMaxima (array, tolerance). The* tolerance used was 2 times the average
602 background intensity. The number of peaks thus obtained was plotted across the
603 width and the plot was fitted to a Gaussian function using Origin(Pro) 2023b. The
604 fitted curve was used as a representative of the arterial coverage per hemisphere.
605 The fit curves obtained from various mice were aligned based on the Gaussian
606 peaks and averaged to get the representative curves for various experimental

607 groups. We considered a region of 1mm (-0.5mm to +0.5 mm) across the Gaussian
608 peak as the collateral zone (watershed). The area under the curve within this region
609 was used as a measure for the extent of the collateral network. 9 hemispheres from
610 9 embryos (e18.5) were analysed per group (control and artery-specific knockout for
611 VegfR2). To test the statistical significance of the differences observed in pial artery
612 coverage (Figure **3E**), a Kolmogorov-Smirnov (KS) test was done. D value= 0.569, p
613 value= 2.2066×10^{-141}. To test the statistical significance of the area under the curve
614 (pial collateral artery network shown in Figure **3F**), an unpaired t-test was done.

615 **AUTHORS CONTRIBUTION**

616 SD conceived the idea and designed the experiments. SK performed intravital
617 imaging of embryos and adults. NS, SG, VS, MD performed other embryonic
618 experiments. SD, SK, NS, SG wrote the manuscript. All authors contributed to
619 editing the manuscript.

620 **ACKNOWLEDGEMENTS**

621 We thank the following facilities for their technical support: Animal Care and
622 Resource Center at NCBS, Mouse Genome Engineering Facility at NCBS, Central
623 Imaging and Flow Cytometry Facility at NCBS. We sincerely thank Dr. Dritan Agalliu
624 (Columbia University) and Dr. Kristy Red-Horse (Stanford University) for generously
625 sharing *Tie2::eGFP::Claudin5* and *Dach1*$^{fl/fl}$ mice respectively.

626 **FUNDING**

627 This work is supported by NCBS/TIFR core funding and DBT/Wellcome Trust India
628 Alliance Intermediate Fellowship to SD (IA/I/20/2/505205). Suraj K is supported by

629 DBT/Wellcome Trust India Alliance Intermediate Fellowship to SD. NS and VS were
630 supported by DBT INSPIRE Scholarship for Higher Education (SHE).

631 **DECLARATION OF INTERESTS**

632 None

633 **REFERENCES**

634 1. Lima, F.O., Furie, K.L., Silva, G.S., Lev, M.H., Camargo, E.C.S., Singhal, A.B.,
635 Harris, G.J., Halpern, E.F., Koroshetz, W.J., Smith, W.S., et al. (2010). The
636 pattern of leptomeningeal collaterals on CT angiography is a strong predictor
637 of long-term functional outcome in stroke patients with large vessel intracranial
638 occlusion. Stroke *41*, 2316–2322. 10.1161/STROKEAHA.110.592303.

639 2. Maas, M.B., Lev, M.H., Ay, H., Singhal, A.B., Greer, D.M., Smith, W.S., Harris,
640 G.J., Halpern, E., Kemmling, A., Koroshetz, W.J., et al. (2009). Collateral
641 vessels on CT angiography predict outcome in acute ischemic stroke. Stroke
642 *40*, 3001–3005. 10.1161/STROKEAHA.109.552513.

643 3. The top 10 causes of death. https://www.who.int/news-room/fact-
644 sheets/detail/the-top-10-causes-of-death.

645 4. Zhang, H., Prabhakar, P., Sealock, R., and Faber, J.E. (2010). Wide genetic
646 variation in the native pial collateral circulation is a major determinant of
647 variation in severity of stroke. Journal of Cerebral Blood Flow & Metabolism
648 *30*, 923–934. 10.1038/jcbfm.2010.10.

649 5. Clayton, J.A., Chalothorn, D., and Faber, J.E. (2008). Vascular endothelial
650 growth factor-a specifies formation of native collaterals and regulates collateral

651 growth in ischemia. Circ Res *103*, 1027–1036.
652 10.1161/CIRCRESAHA.108.181115.

653 6. Lucitti, J.L., MacKey, J.K., Morrison, J.C., Haigh, J.J., Adams, R.H., and Faber,
654 J.E. (2012). Formation of the collateral circulation is regulated by vascular
655 endothelial growth factor-a and a disintegrin and metalloprotease family
656 members 10 and 17. Circ Res *111*, 1539–1550.
657 10.1161/CIRCRESAHA.112.279109.

658 7. Lucitti, J.L., Sealock, R., Buckley, B.K., Zhang, H., Xiao, L., Dudley, A.C., and
659 Faber, J.E. (2016). Variants of Rab GTPase-Effector Binding Protein-2 Cause
660 Variation in the Collateral Circulation and Severity of Stroke. Stroke *47*, 3022–
661 3031. 10.1161/STROKEAHA.116.014160.

662 8. Chalothorn, D., Clayton, J.A., Zhang, H., Pomp, D., and Faber, J.E. (2007).
663 Collateral density, remodeling, and VEGF-A expression differ widely between
664 mouse strains. Physiol Genomics *30*, 179–191.
665 10.1152/physiolgenomics.00047.2007.

666 9. Das, S., Goldstone, A.B., Wang, H., Farry, J., D'Amato, G., Paulsen, M.J.,
667 Eskandari, A., Hironaka, C E., Phansalkar, R., Sharma, B., et al. (2019). A
668 Unique Collateral Artery Development Program Promotes Neonatal Heart
669 Regeneration. Cell *176*, 1128-1142.e18. 10.1016/J.CELL.2018.12.023.

670 10. Perovic, T., Hollfinger, I., Mayer, S., Lips, J., Dopatka, M., Harms, C., and
671 Gerhardt, H. (2023). Pial collaterals develop through mosaic colonization of
672 capillaries by arterial and microvascular endothelial cells. bioRxiv,
673 2023.10.09.561542. 10.1101/2023.10.09.561542.

674 11. Gabhann, F. Mac, and Peirce, S.M. (2010). Collateral Capillary Arterialization
675 following Arteriolar Ligation in Murine Skeletal Muscle. Microcirculation *17*,
676 333–347. 10.1111/J.1549-8719.2010.00034.X.

677 12. Jamaiyar, A., Juguilon, C., Wan, W., Richardson, D., Chinchilla, S., Gadd, J.,
678 Enrick, M., Wang, T., McCabe, C., Wang, Y., et al. (2022). The essential role
679 for endothelial cell sprouting in coronary collateral growth. J Mol Cell Cardiol
680 *165*, 158–171. 10.1016/j.yjmcc.2022.01.005.

681 13. Arolkar, G., Kumar, S.K., Wang, H., Gonzalez, K.M., Kumar, S., Bishnoi, B.,
682 Rios Coronado, P.E., Woo, Y.J., Red-Horse, K., and Das, S. (2023).
683 Dedifferentiation and Proliferation of Artery Endothelial Cells Drive Coronary
684 Collateral Development in Mice. Arterioscler Thromb Vasc Biol *43*, 1455–1477.
685 10.1161/ATVBAHA.123.319319.

686 14. Chang, A.H., Raftrey, B.C., D'Amato, G., Surya, V.N., Poduri, A., Chen, H.I.,
687 Goldstone, A.B., Woo, J., Fuller, G.G., Dunn, A.R., et al. (2017). DACH1
688 stimulates shear stress-guided endothelial cell migration and coronary artery
689 growth through the CXCL12-CXCR4 signaling axis. Genes Dev *31*, 1308–
690 1324. 10.1101/GAD.301549.117/-/DC1.

691 15. Chen, H.I., Sharma, B., Akerberg, B.N., Numi, H.J., Kivelä, R., Saharinen, P.,
692 Aghajanian, H., McKay, A.S., Bogard, P.E., Chang, A.H., et al. (2014). The
693 sinus venosus contributes to coronary vasculature through VEGFC-stimulated
694 angiogenesis. Development *141*, 4500–4512. 10.1242/dev.113639.

695 16. Scott Budinger, G.R., Duranteau, J., Chandel, N.S., and Schumacker, P.T.
696 (1998). Hibernation during Hypoxia in Cardiomyocytes ROLE OF

697 MITOCHONDRIA AS THE O 2 SENSOR*. Journal of Biological Chemistry
698 *273*, 3320–3326. 10.1074/jbc.273.6.3320.

699 17. Rink, C., and Khanna, S. (2011). Significance of Brain Tissue Oxygenation and
700 the Arachidonic Acid Cascade in Stroke. https://home.liebertpub.com/ars *14*,
701 1889–1903. 10.1089/ARS.2010.3474.

702 18. Mannion, J.D., Buckman, P.D., Magno, M.G., and Dimeo, F. (1992). Collateral
703 blood flow from skeletal muscle to normal myocardium. Journal of Surgical
704 Research *53*, 578–587. 10.1016/0022-4804(92)90258-2.

705 19. Crissinger, K.D., and Neil Granger, D. (1988). Characterization of Intestinal
706 Collateral Blood Flow in the Developing Piglet. Pediatr Res *24*, 473–476.
707 10.1203/00006450-198810000-00011.

708 20. Kochi, T., Imai, Y., Takeda, A., Watanabe, Y., Mori, S., Tachi, M., and
709 Kodama, T. (2013). Characterization of the Arterial Anatomy of the Murine
710 Hindlimb: Functional Role in the Design and Understanding of Ischemia
711 Models. PLoS One *8*, e84047. 10.1371/JOURNAL.PONE.0084047.

712 21. Gao, Y., Aravind, S., Patel, N.S., Fuglestad, M.A., Ungar, J.S., Mietus, C.J., Li,
713 S., Casale, G.P., Pipinos, I.I., and Carlson, M.A. (2020). Collateral
714 Development and Arteriogenesis in Hindlimbs of Swine After Ligation of
715 Arterial Inflow. Journal of Surgical Research *249*, 168–179.
716 10.1016/J.JSS.2019.12.005.

717 22. He, L., Liu, Q., Hu, T., Huang, X., Zhang, H., Tian, X., Yan, Y., Wang, L.,
718 Huang, Y., Miquerol, L., et al. (2016). Genetic lineage tracing discloses

719 arteriogenesis as the main mechanism for collateral growth in the mouse
720 heart. Cardiovasc Res *109*, 419–430. 10.1093/CVR/CVW005.

721 23. Raftrey, B., Williams, I.M., Rios Coronado, P.E., Fan, X., Chang, A.H., Zhao,
722 M., Roth, R., Trimm, E., Racelis, R., D'amato, G., et al. (2021). Dach1 Extends
723 Artery Networks and Protects Against Cardiac Injury. Circ Res *129*, 702–716.
724 10.1161/CIRCRESAHA.120.318271.

725 24. Zhang, H., Chalothorn, D., and Faber, J.E. (2019). Collateral Vessels Have
726 Unique Endothelial and Smooth Muscle Cell Phenotypes. International Journal
727 of Molecular Sciences 2019, Vol. 20, Page 3608 *20*, 3608.
728 10.3390/IJMS20153608.

729 25. Stanca Melincovici, C., Boşca, A.B., Şuşman, S., Mărginean, M., Mihu, C.,
730 Istrate, M., Moldovan, I.-M., Roman, A.L., and Mihu, C.M. (2018). Vascular
731 endothelial growth factor (VEGF)-key factor in normal and pathological
732 angiogenesis. Rom J Morphol Embryol *59*.

733 26. Miquerol, L., Thireau, J., Bideaux, P., Sturny, R., Richard, S., and Kelly, R.G.
734 (2015). Endothelial plasticity drives arterial remodeling within The endocardium
735 after myocardial infarction. Circ Res *116*, 1765–1771.
736 10.1161/CIRCRESAHA.116.306476.

737 27. Miquerol, L., Meysen, S., Mangoni, M., Bois, P., van Rijen, H.V.M., Abran, P.,
738 Jongsma, H., Nargeot, J., and Gros, D. (2004). Architectural and functional
739 asymmetry of the His–Purkinje system of the murine heart. Cardiovasc Res
740 *63*, 77–86. 10.1016/j.cardiores.2004.03.007.

741 28. Knowland, D., Arac, A., Sekiguchi, K.J., Hsu, M., Lutz, S.E., Perrino, J.,
742 Steinberg, G.K., Barres, B.A., Nimmerjahn, A., and Agalliu, D. (2014).
743 Stepwise Recruitment of Transcellular and Paracellular Pathways Underlies
744 Blood-Brain Barrier Breakdown in Stroke. Neuron *82*, 603–617.
745 10.1016/j.neuron.2014.03.003.

746 29. Lutz, S.E., Smith, J.R., Kim, H., Bates, J.M., Gandhi, S.P., and Agalliu, D.
747 (2017). Caveolin1 Is Required for Th1 Cell Infiltration, but Not Tight Junction
748 Remodeling, at the Blood-Brain Barrier in Autoimmune Neuroinflammation.
749 CellReports *21*, 2104–2117. 10.1016/j.celrep.2017.10.094.

750 30. Holtmaat, A.J.G.D., Trachtenberg, J.T., Wilbrecht, L., Shepherd, G.M., Zhang,
751 X., Knott, G.W., and Svoboda, K. (2005). Transient and Persistent Dendritic
752 Spines in the Neocortex In Vivo. Neuron *45*, 279–291.
753 10.1016/j.neuron.2005.01.003.

754

755

Main figures and figure legends

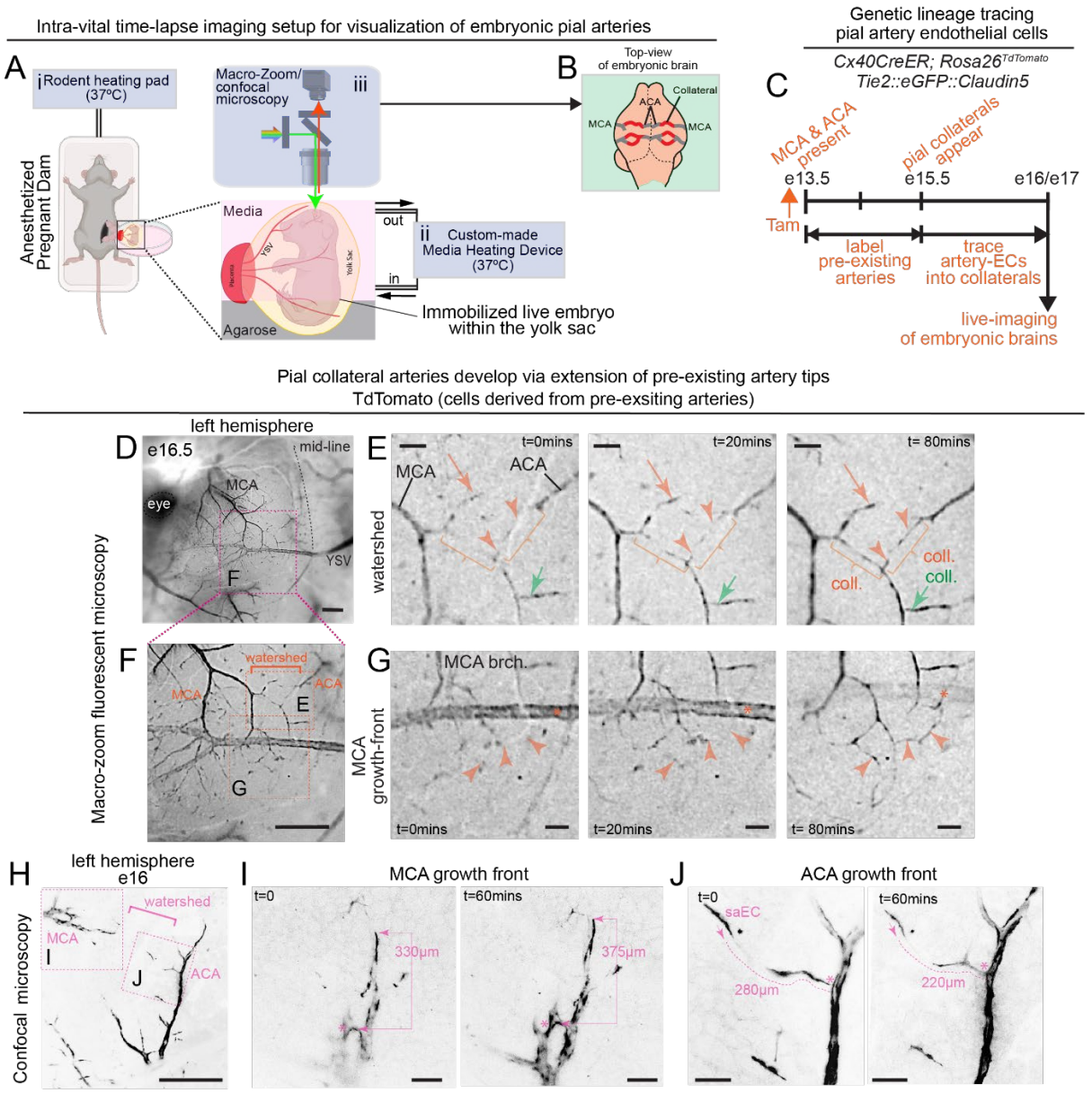

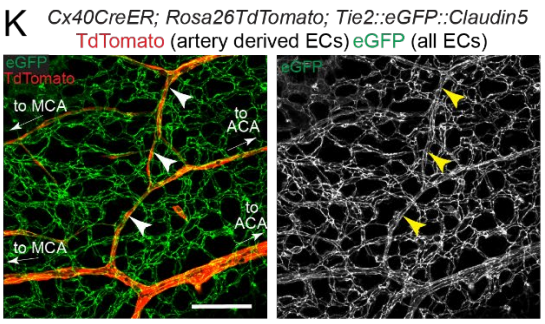

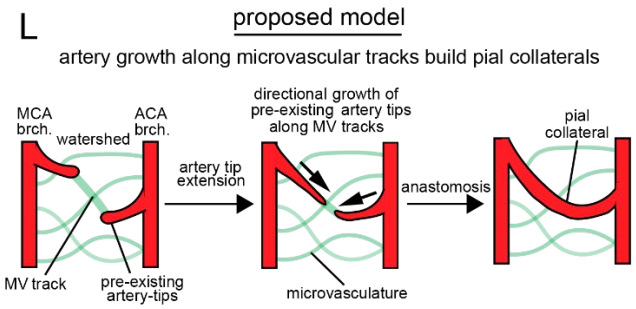

759 **Figure 1: Live imaging developing pial vasculature**

760 (**A**) Intra-vital imaging set up to visualize the developing pial vasculature in mouse
761 embryos. **i** heating pad to maintain body temperature of anaesthetized pregnant
762 mouse at 37°C. **ii** custom built media heating device which also circulates dissection
763 media at 37°C **iii** shows macro-zoom or confocal microscopy performed on live,
764 immobilized embryos.

765 (**B**) Representative schematic of an embryonic brain. Grey and Red show cerebral
766 arteries and pial collaterals respectively.

767 (**C**) Experimental design to genetically label and trace the dynamics of pre-existing
768 artery endothelial cells in a developing pial layer.

769 (**D**-**G**) Images obtained through macro-zoom fluorescent microscopy of e16.5
770 embryos. In black are cells derived from pre-existing artery endothelial cells. Images
771 were taken by focusing in and out to capture the entire curvature of the embryonic
772 brain. **D** shows an entire left hemisphere. **E** represents watershed region spanned
773 with MCA and ACA artery tips and imaged at time=0 minutes, 20 minutes and 80
774 minutes respectively. Arrows and arrowheads show growing ends of pre-existing
775 artery tips from MCA and ACA. Brackets mark regions where collaterals appear. **F**
776 shows inset in **D**. **E** and **G** show insets in **F**. **G** represents the MCA growth front
777 imaged at time=0 minutes, 20 minutes and 80 minutes respectively. * shows a
778 superficial yolk sac vessel which photobleaches with time.

779 (**H**-**J**) Images obtained through confocal microscopy from e16 embryos. **H** shows pial
780 watershed and the cerebral arteries spanning the watershed. **I**, **J** show MCA and
781 ACA growth fronts respectively imaged at time=0 minutes and 60 minutes. In black
782 are cells derived from pre-existing artery endothelial cells. Images are maximum

783 intensity projections from 50 optical slices and capture the entire width of the artery.
784 Dotted line shows the length of micro-vessel connecting the single artery cell to the
785 base of the emergent sprout. * represents an internal landmark from where the
786 length measurements were done.

787 (**K**) Confocal images of e17 pial layer showing presence of TdTomato$^+$ pre-existing
788 artery endothelial cells (arrowheads) on GFP$^+$ microvascular tracks. Arrowheads
789 point to TdTomato$^+$ artery cells (red) on microvascular tracks (green).

790 (**L**) A model proposing extension of artery tips along microvascular tracks which
791 leads to pial collateral formation during embryogenesis. Grey arrows point to the
792 direction of artery tip elongation. MCA, Middle cerebral artery; ACA, Anterior cerebral
793 artery; e, embryonic day; Tam, Tamoxifen; EC, endothelial cell; YSV, yolk sac
794 vessel; brch., branch; coll, collateral; MV, microvascular. Scale bars: **D**, **F** 1mm; **E**, **G**
795 200 μm; **H**, 500 μm; **I**, **J**, **K** 100 μm.

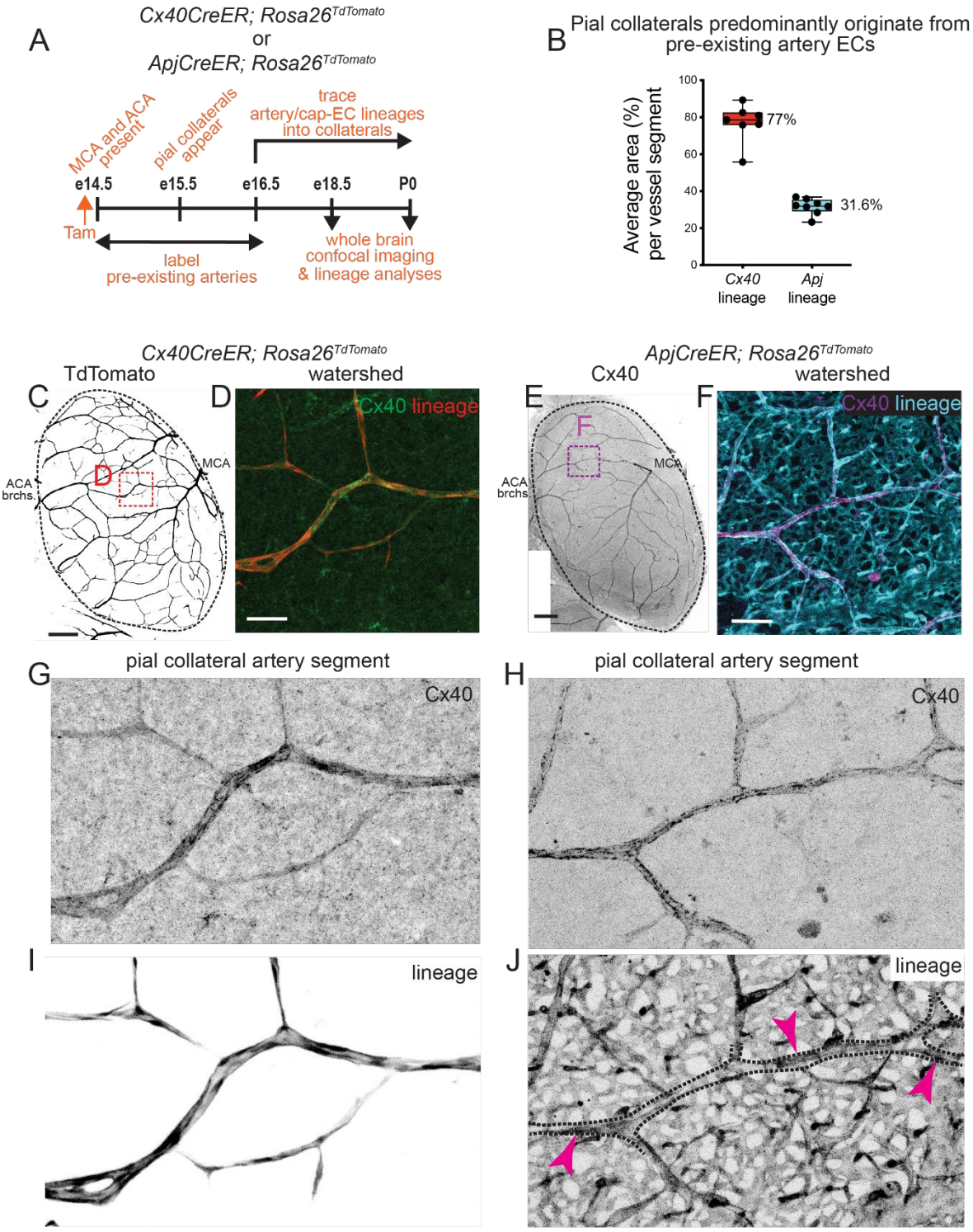
A
Cx40CreER; Rosa26TdTomato
or
ApjCreER; Rosa26TdTomato
MCA and ACA present
pial collaterals appear
trace artery/cap-EC lineages into collaterals
e14.5
e15.5
e16.5
e18.5
P0
Tam
label pre-existing arteries
whole brain confocal imaging & lineage analyses
B
Pial collaterals predominantly originate from pre-existing artery ECs
Average area (%) per vessel segment
100
80
60
40
20
0
77%
31.6%
Cx40 lineage
Apj lineage
Cx40CreER; Rosa26TdTomato
TdTomato
watershed
C
D
ACA brchs
MCA
Cx40 lineage
ApjCreER; Rosa26TdTomato
Cx40
watershed
E
F
ACA brchs
MCA
Cx40 lineage
G
pial collateral artery segment
Cx40
H
pial collateral artery segment
Cx40
I
lineage
J
lineage

800 **Figure 2: Cellular origin of pial collaterals**

801 (**A**) Experimental design to assess lineage contribution from artery ECs and capillary
802 ECs towards pial collaterals at e18.5/ P0.
803 (**B**) Graph shows the average percent area of collateral segments covered with
804 TdTomato^{+} cells.
805 (**C**) Representative image of whole right hemisphere from *Cx40CreER*;
806 *Rosa26^{TdTomato}* e18.5 embryos. Black shows TdTomato^{+} arteries.
807 (**D**) Boxed region of interest with a collateral segment from the watershed area
808 shown in **C**. The pial collateral is lineage traced for artery ECs (red) and
809 immunostained with Cx40 (green).
810 **(E**) Representative image of whole right hemisphere from *ApjCreER*; *Rosa26^{TdTomato}*
811 e18.5 embryos. Black shows Cx40 immunostaining.
812 (**F**) Boxed region of interest with a collateral segment from the watershed area
813 shown in **E**. The pial collateral is lineage traced for capillary ECs (red) and
814 immunostained with Cx40 (green).
815 (**G**, **I**) Collateral segment from **D** is (**G**) immunostained for Cx40 and (**I**) lineage
816 traced with TdTomato.
817 (**H**, **J**) Collateral segment from **F** is (**H**) immunostained for Cx40 and (**J**) lineage
818 traced with TdTomato. Arrowheads point to TdTomato^{+} cells from Apj^{+} lineage on the
819 collateral segment. e, embryonic day, P, postnatal day; MCA, Middle cerebral artery;
820 ACA, Anterior cerebral artery; brch., branch; EC, endothelial cell. Scale bars: **C** and
821 **E**, 500μm; **E** and **F**, 100μm
822

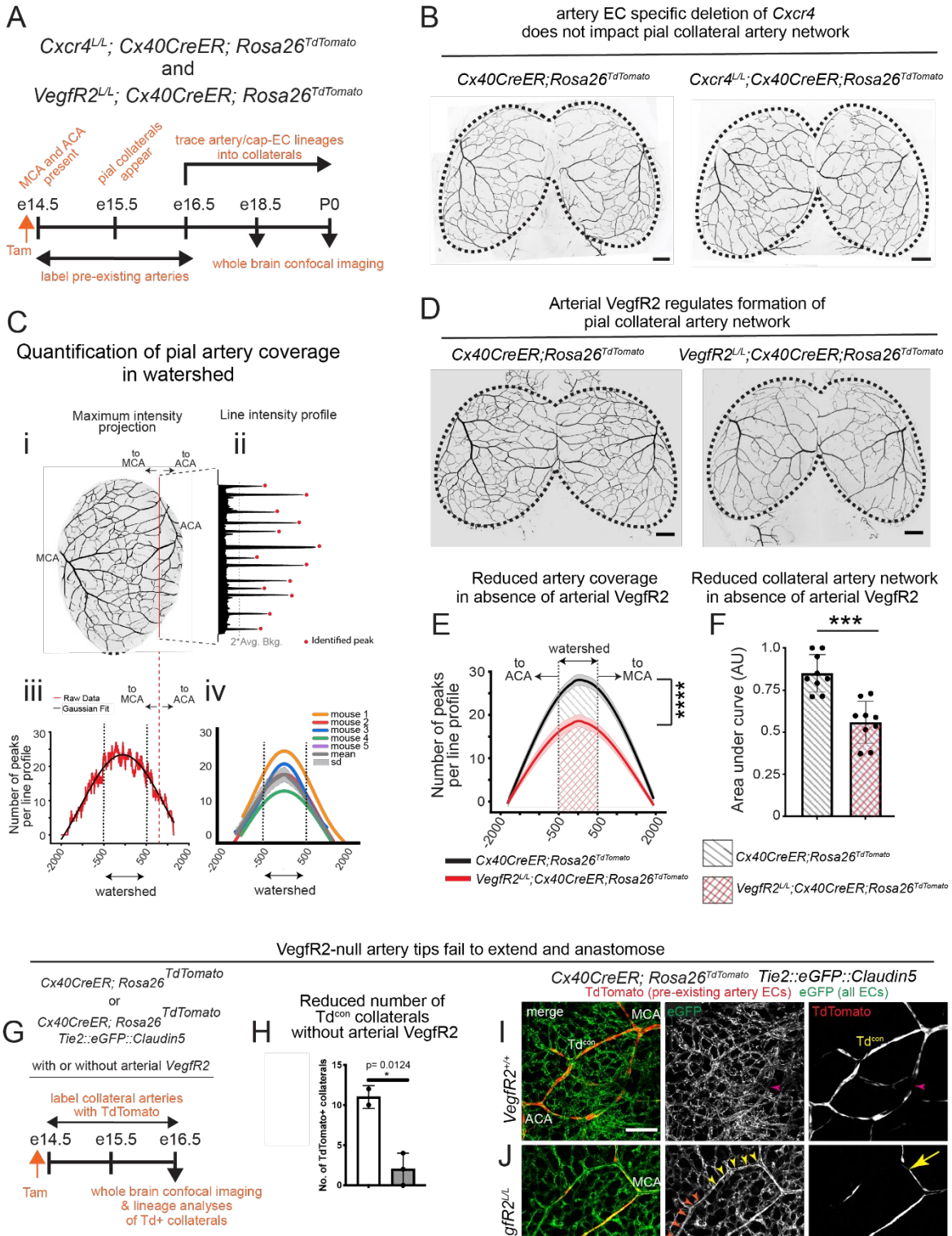
A
Cxcr4L/L; Cx40CreER; Rosa26TdTomato
and
VegfR2L/L; Cx40CreER; Rosa26TdTomato
MCA and ACA present
pial collaterals appear
trace artery/cap-EC lineages into collaterals
e14.5
e15.5
e16.5
e18.5
P0
Tam
label pre-existing arteries
whole brain confocal imaging
B
artery EC specific deletion of Cxcr4 does not impact pial collateral artery network
Cx40CreER;Rosa26TdTomato
Cxcr4L/L;Cx40CreER;Rosa26TdTomato
C
Quantification of pial artery coverage in watershed
Maximum intensity projection
Line intensity profile
i
ii
to MCA
to ACA
ACA
MCA
2*Avg. Bkg.
Identified peak
iii
iv
Raw Data
Gaussian Fit
Number of peaks per line profile
watershed
mouse 1
mouse 2
mouse 3
mouse 4
mouse 5
mean
sd
D
Arterial VegfR2 regulates formation of pial collateral artery network
Cx40CreER;Rosa26TdTomato
VegfR2L/L;Cx40CreER;Rosa26TdTomato
Reduced artery coverage in absence of arterial VegfR2
Reduced collateral artery network in absence of arterial VegfR2
E
F
watershed
to ACA
to MCA
****
***
Number of peaks per line profile
Area under curve (AU)
Cx40CreER;Rosa26TdTomato
VegfR2L/L;Cx40CreER;Rosa26TdTomato
VegfR2-null artery tips fail to extend and anastomose
Cx40CreER; Rosa26TdTomato
or
Cx40CreER; Rosa26TdTomato
Tie2::eGFP::Claudin5
with or without arterial VegfR2
G
label collateral arteries with TdTomato
e14.5
e15.5
e16.5
Tam
whole brain confocal imaging & lineage analyses of Td+ collaterals
H
Reduced number of Tdcon collaterals without arterial VegfR2
p= 0.0124
No. of TdTomato+ collaterals
Cx40CreER; Rosa26TdTomato Tie2::eGFP::Claudin5
TdTomato (pre-existing artery ECs) eGFP (all ECs)
I
J
merge
eGFP
TdTomato
Tdcon
MCA
ACA
VegfR2+/+
VegfR2L/L

823

824

825

826 **Figure 3: VegfR2-dependent formation of pial collateral arteries**

827 (**A**) Experimental design to lineage label and trace pre-existing artery endothelial
828 cells in pial layer, with or without arterial *VegfR2* and *Cxcr4* at e18.5/ P0.

829 (**B**) Representative confocal images of whole brains with and without arterial *Cxcr4*.
830 Black shows pre-existing artery endothelial cells. Control= 8, artery specific knockout
831 for *Cxcr4*= 13.

832 (**C**) Summary of method for quantifying complex pial artery coverage across the
833 entire brain and in the watershed.

834 (**D**) Confocal images of whole brains with and without arterial *VegfR2*. Black shows
835 pre-existing artery endothelial cells.

836 (**E**) Quantification of overall pial artery coverage without arterial *VegfR2* quantified
837 using method shown in **C**. KS test performed on the distribution generated D value=
838 0.569, p value= 2.2066×10^{-141}.

839 (**F**) Quantification of pial collateral artery network without arterial *VegfR2* quantified
840 using method shown in **C**. Unpaired t-test, p=0.0001.

841 (**G-J**) Analysis of e16.5 brains. (**G**) Experimental design. (**H**) Quantification of pial
842 collateral arteries continuously populated with TdTomato^{+} artery cells. (**I**, **J**) Confocal
843 images of pial watershed region showing TdTomato-continuous pial collateral
844 arteries (Td^{con}) in red and microvasculature in green. Arrowheads show part of
845 microvascular track not occupied by TdTomato^{+} artery cell, arrows point to artery tips
846 on microvascular tracks. MCA, Middle cerebral artery; ACA, Anterior cerebral artery;
847 e, embryonic day; P, postnatal day; Tam, Tamoxifen; EC, endothelial cell; Td^{con},

848 TdTomato-continuous; AU, Arbitrary Unit. Scale bars: **B**, 500μm; **D**, 500μm; **I**, **J**,

849 100μm.

850

851

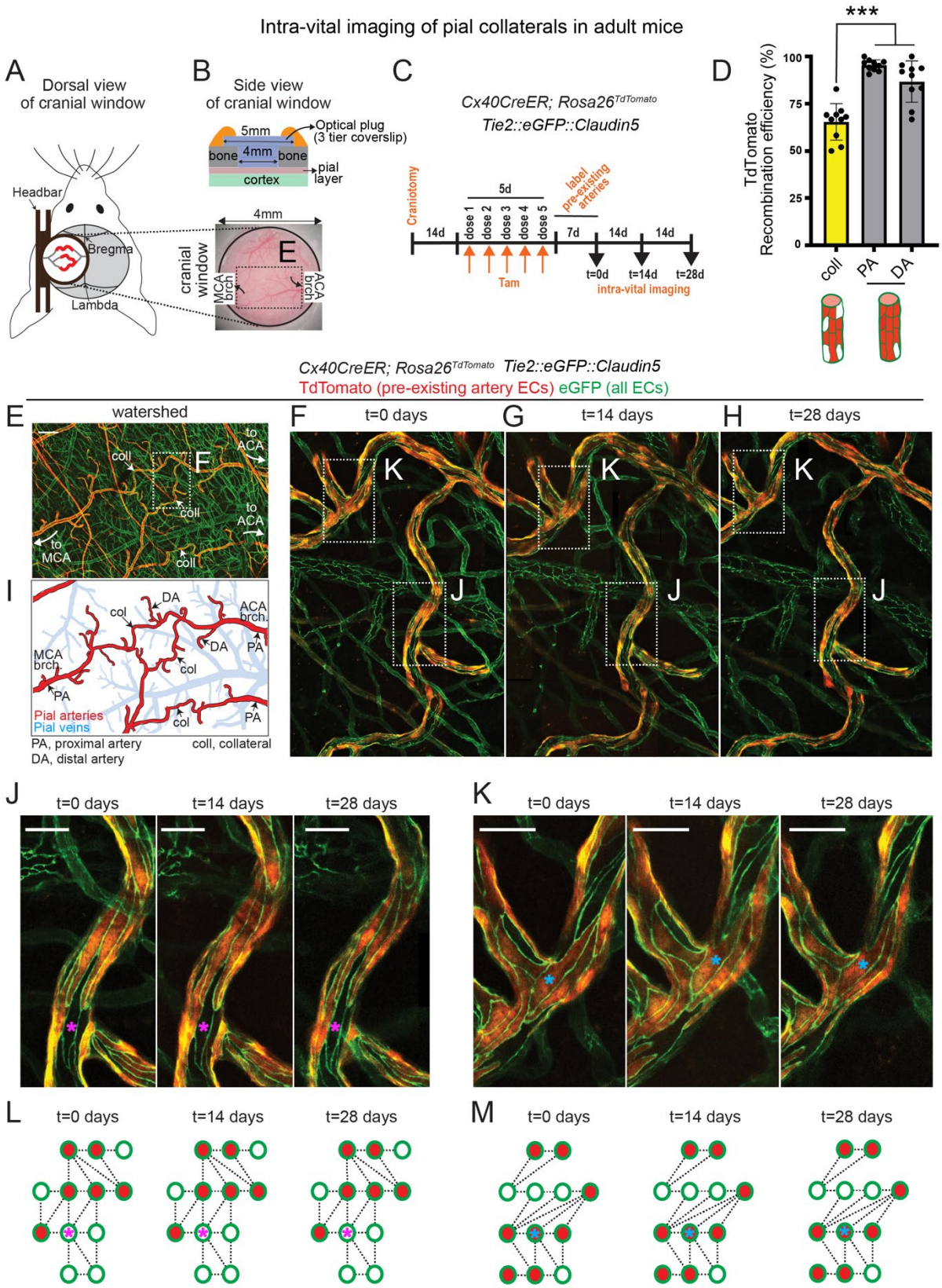
Intra-vital imaging of pial collaterals in adult mice
A
Dorsal view of cranial window
Headbar
Bregma
Lambda
B
Side view of cranial window
5mm
Optical plug (3 tier coverslip)
bone
4mm
bone
pial layer
cortex
4mm
cranial window
MCA brch
ACA brch
E
C
Cx40CreER; Rosa26TdTomato
Tie2::eGFP::Claudin5
Craniotomy
5d
label pre-existing arteries
14d
dose 1
dose 2
dose 3
dose 4
dose 5
7d
14d
14d
Tam
t=0d
t=14d
t=28d
intra-vital imaging
D
***
TdTomato Recombination efficiency (%)
100
75
50
25
0
coll
PA
DA
Cx40CreER; Rosa26TdTomato Tie2::eGFP::Claudin5
TdTomato (pre-existing artery ECs) eGFP (all ECs)
E
watershed
coll
F
to ACA
coll
to ACA
to MCA
coll
I
DA
col
ACA brch.
DA
PA
MCA brch.
col
PA
Pial arteries
Pial veins
col
PA
PA, proximal artery
DA, distal artery
coll, collateral
F
t=0 days
G
t=14 days
H
t=28 days
K
J
K
J
K
J
J
t=0 days
t=14 days
t=28 days
K
t=0 days
t=14 days
t=28 days
L
t=0 days
t=14 days
t=28 days
M
t=0 days
t=14 days
t=28 days

852

853

854

855 **Figure 4: Longitudinal live imaging of adult pial collaterals**

856 (**A**, **B**) Dorsal and side view of the cranial window created on adult mouse head.

857 (**C**) Experimental design for longitudinal imaging of pial vasculature in adult mice.

858 (**D**) Quantification of TdTomato reporter recombination in pial collateral arteries and
859 different segments of cerebral arteries. One-way ANOVA, Tukey test, p=0.0001

860 (**E**-**K**) Images of pial watershed with pre-existing artery endothelial cells labelled in
861 TdTomato (red) and all endothelial cells labelled in eGFP (green).

862 (**E**) Confocal images from optical window created for longitudinal imaging of
863 *Cx40CreER; Rosa26^{TdTomato}; Tie2::eGFP::Claudin5* mice. The image shows both pial
864 and dural vessels.

865 (**F**-**K**) Confocal images of pial collateral arteries from cranial window shown in E,
866 across 3 timepoints, each 2 weeks apart. (**I**) Pial layer segmented out from **E**. red
867 and blue show pial arteries and veins respectively. **J**, **K** are the insets shown in **F**-**H**.

868 (**L**, **M**) Cellular distribution of TdTomato+ artery cells and eGFP+ endothelial cells in
869 collateral artery segments shown in **J** and **K** respectively. * represents a reference
870 cell. MCA, middle cerebral artery; ACA, anterior cerebral artery; d, days; Tam,
871 Tamoxifen; PA, proximal artery; DA, distal artery; coll, collateral; brch., branch; EC,
872 endothelial cell. Scale bars: **E**, 1mm; **J**, **K** 25μm

873

Intra-vital imaging of VegfR2 deficient pial collaterals in adult mice

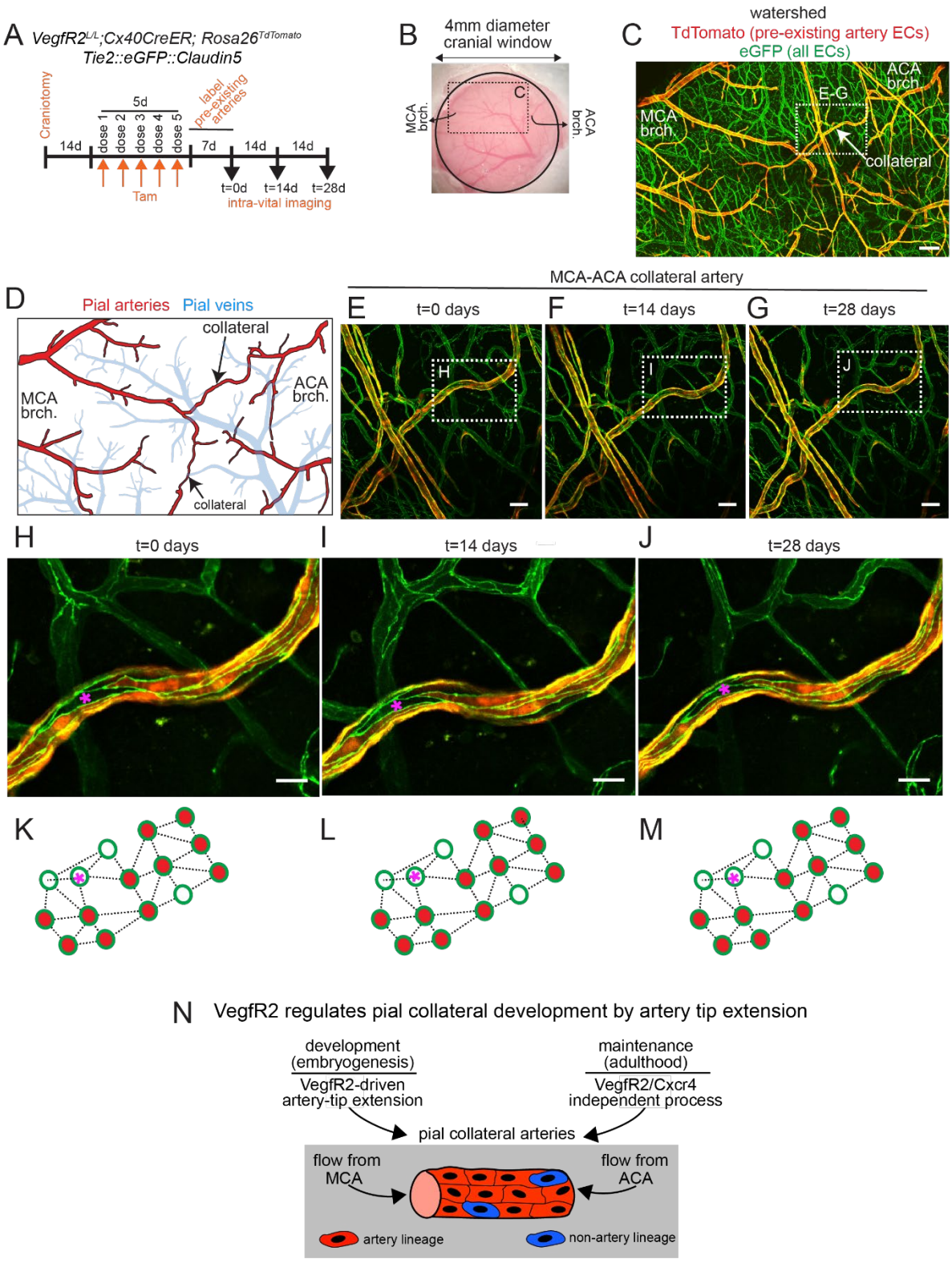

N VegfR2 regulates pial collateral development by artery tip extension

874

875

876

877 **Figure 5: Analyses of role of arterial VegfR2 in pial collateral maintenance**

878 **(A)** Experimental design to visualize artery cell dynamics in pial layer of adult mice
879 without arterial *VegfR2*.

880 (**B**) White-field image of cranial window.

881 (**C**) Confocal image of cranial window created in mice without arterial *VegfR2*. Red
882 shows all artery cells, green shows all endothelial cells.

883 (**D**) Pial layer segmented out from C shows pial arteries and veins in red and blue.

884 (**E**-**G**) Confocal images of collateral artery from three timepoints, each 2 weeks apart.

885 (**H**-**J**) Confocal images of collateral artery segments shown in E-G.

886 (**K**-**M**) Cellular distribution of TdTomato+ artery cells and eGFP^{+} endothelial cells in
887 collateral artery segments shown in **H**-**J**. * represents a reference cell.

888 (**N**) Schematic summarizing the role of arterial VegfR2 in development and
889 maintenance of pial collateral arteries. While arterial VegfR2 facilitates tip extension
890 of pre-existing arteries during development, it is dispensable for pial collateral
891 maintenance in adulthood. Pial collaterals, both in developing and mature brains, are
892 majorly populated by endothelial cells of artery-lineage. MCA, middle cerebral artery;
893 ACA, anterior cerebral artery; d, days; Tam, Tamoxifen; EC, endothelial cell; brch.,
894 branch. Scale bars: **C**, 1mm; **E**-**G**, 50μm; **H**-**J**, 20μm.

895

896

897

898

Supplementary figures and figure legends

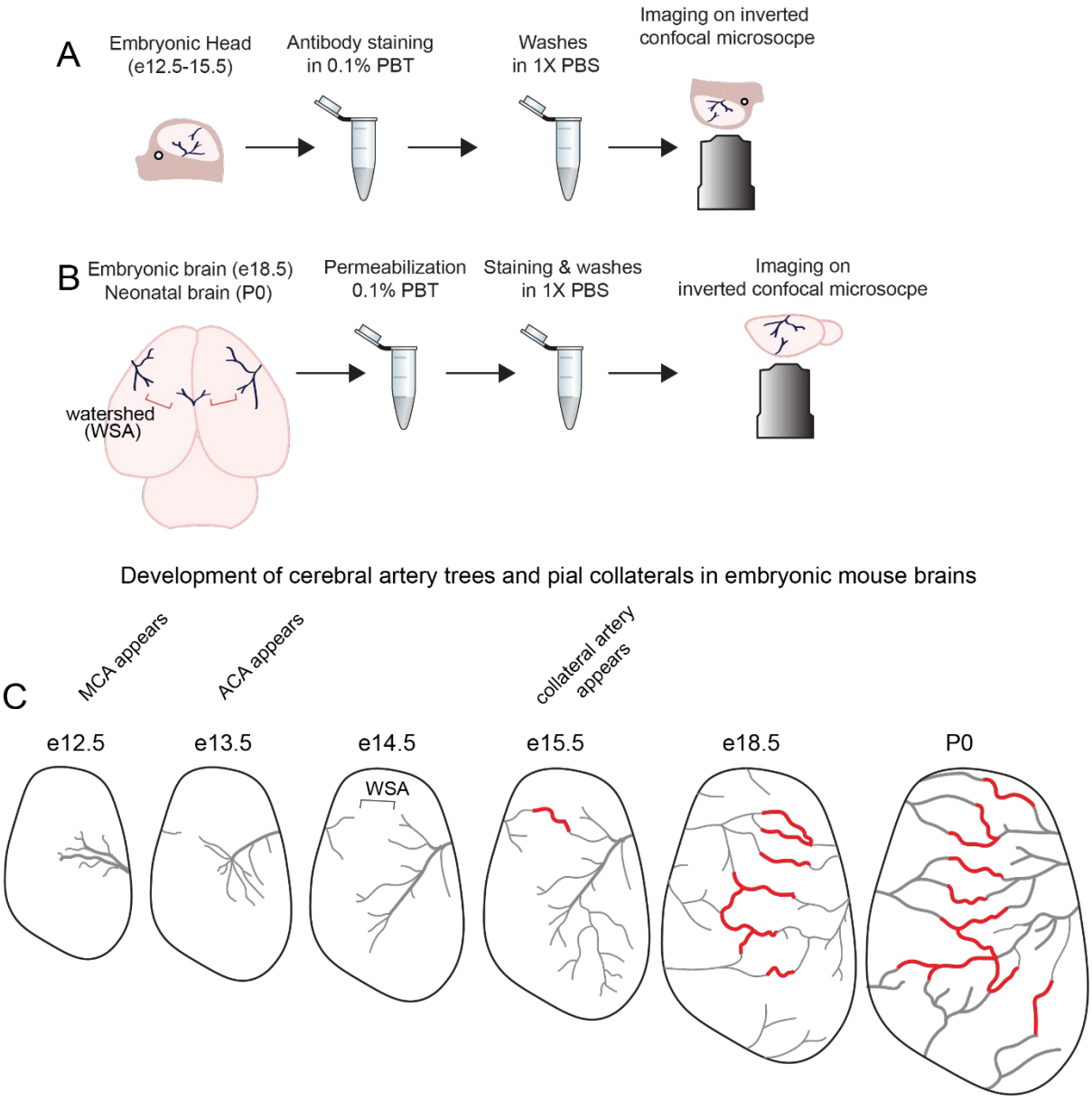

906 **Supplemental Figure 1: Visualization of pial arteries and collateral arteries**

907 Schematic summarizes key steps of immunostaining methods used to image pial
908 artery network in (**A**) mouse embryonic heads and (**B**) mouse embryonic/neonatal
909 brains with confocal microscope. (**C**) Schematic shows findings from **A** and **B** in one
910 hemisphere. Grey represents cerebral arteries, Red represents collateral artery
911 connections between cerebral arteries. Brackets show watershed area (WSA), MCA
912 appears at e12.5, ACA appears at e13.5, and the foremost pial collateral arteries
913 appear at e15.5. These pial collaterals then increase in number till e18.5/P0. e,
914 embryonic; P, postnatal day; MCA, middle cerebral artery; ACA, anterior cerebral
915 artery.

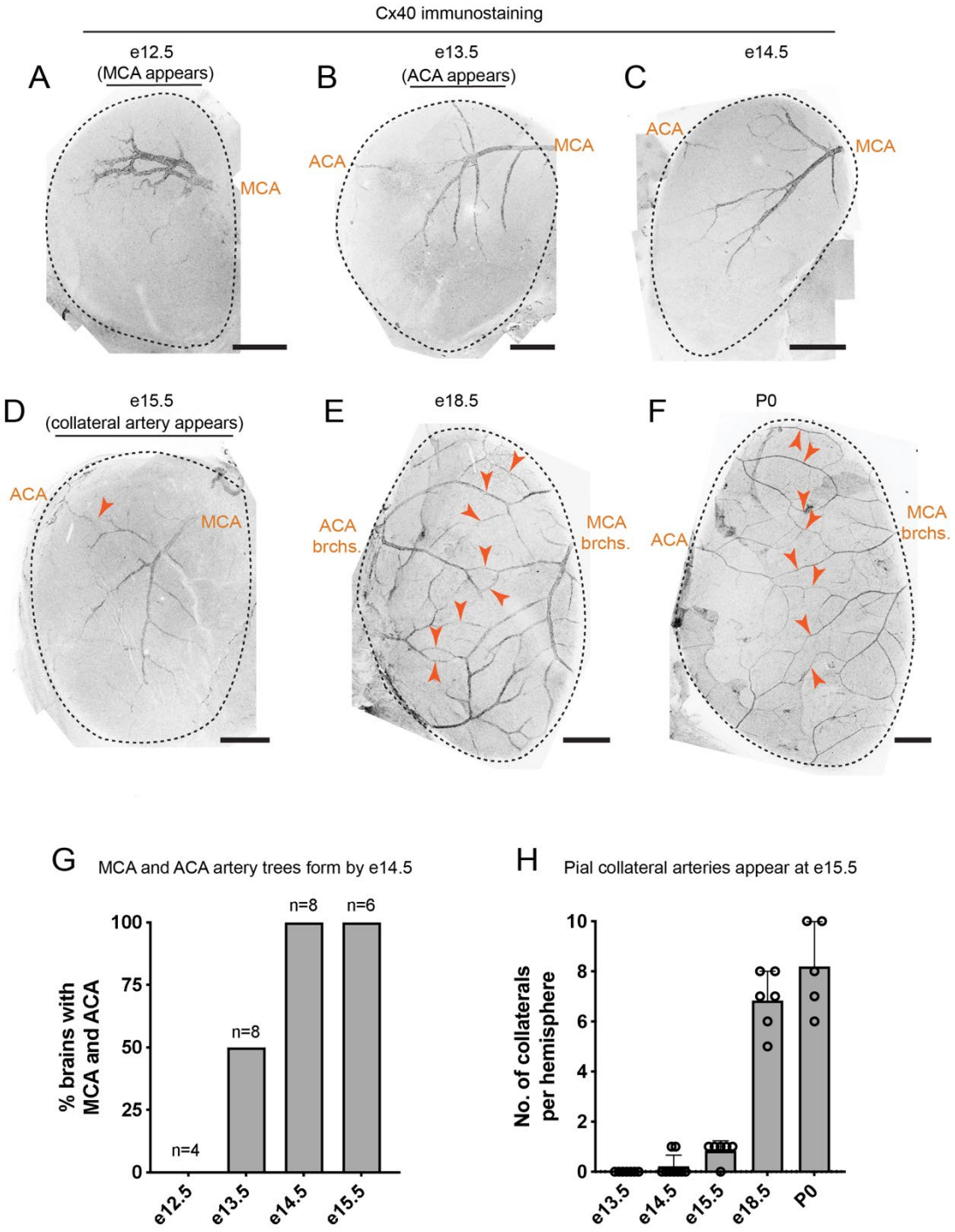
Cx40 immunostaining
A
e12.5
(MCA appears)
MCA
B
e13.5
(ACA appears)
ACA
MCA
C
e14.5
ACA
MCA
D
e15.5
(collateral artery appears)
ACA
MCA
E
e18.5
ACA
brchs.
MCA
brchs.
F
P0
ACA
MCA
brchs.
G
MCA and ACA artery trees form by e14.5
% brains with
MCA and ACA
100
75
50
25
0
n=4
n=8
n=8
n=6
e12.5
e13.5
e14.5
e15.5
H
Pial collateral arteries appear at e15.5
No. of collaterals
per hemisphere
10
8
6
4
2
0
e13.5
e14.5
e15.5
e18.5
P0

920 **Supplemental Figure 2: Detection of pial collaterals with whole brain**
921 **immunostaining**

922 (**A**-**F**) Representative images of right hemispheres from developing mouse embryos
923 immunostained for Cx40. Cx40 marks all arteries. MCA appears at e12.5, ACA
924 appears at e13.5 and collaterals between MCA and ACA appear at e15.5.
925 Arrowheads point to collateral arteries between MCA and ACA. (**G**) Quantification of
926 Cx40 immunostained brains from different developmental stages reveals that both
927 MCA and ACA have formed by e14.5. (**H**) Quantification of $Cx40^{+}$ collateral arteries
928 per hemisphere shows that the first pial collaterals appear at e15.5. e, embryonic; P,
929 postnatal day; MCA, middle cerebral artery; ACA, anterior cerebral artery; brch.,
930 branch. Scale bars: 500µm

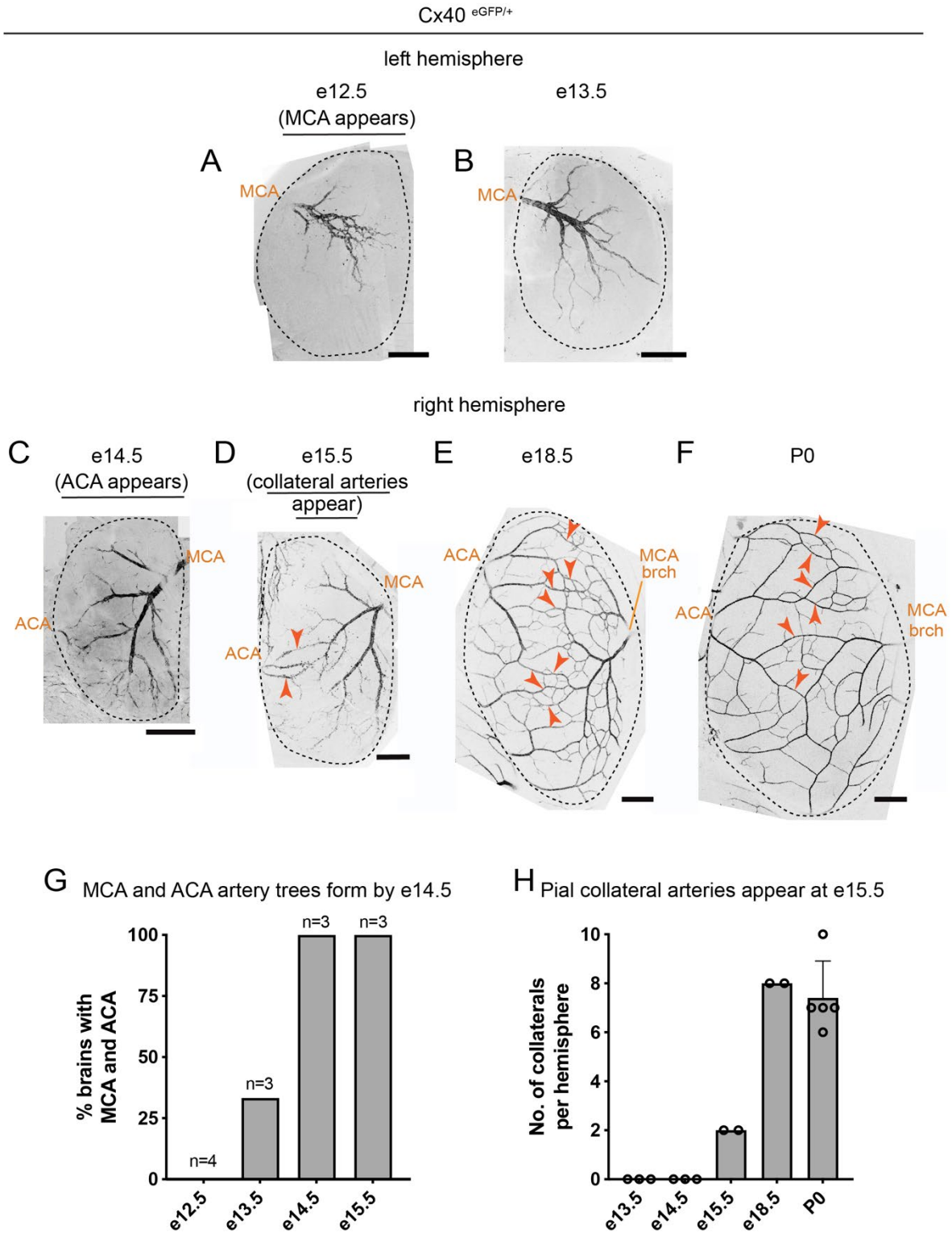
Cx40 eGFP/+
left hemisphere
e12.5
(MCA appears)
e13.5
A
B
MCA
MCA
right hemisphere
C
e14.5
(ACA appears)
D
e15.5
(collateral arteries
appear)
E
e18.5
F
P0
MCA
ACA
MCA
ACA
ACA
MCA
brch
ACA
MCA
brch
G
MCA and ACA artery trees form by e14.5
% brains with
MCA and ACA
100
75
50
25
0
n=4
n=3
n=3
n=3
e12.5
e13.5
e14.5
e15.5
H
Pial collateral arteries appear at e15.5
No. of collaterals
per hemisphere
10
8
6
4
2
0
e13.5
e14.5
e15.5
e18.5
P0

935 **Supplemental Figure 3: Detection of pial collaterals with *Cx40* reporter activity**

936 (**A**-**F**) Representative images of brains from developing *Cx40*$^{eGFP/+}$ mouse embryos.
937 Cx40 marks all arteries. MCA appears at e12.5, ACA appears at e14.5 and
938 collaterals between MCA and ACA appear at e15.5. Arrowheads point to collateral
939 arteries between MCA and ACA. (**G**) Quantification of *Cx40*$^{eGFP/+}$ brains from
940 different developmental stages reveals that both MCA and ACA have formed by
941 e14.5. (**H**) Quantification of eGFP^{+} collateral arteries per hemisphere shows that the
942 first pial collaterals appear at e15.5. e, embryonic; P, postnatal day; MCA, middle
943 cerebral artery; ACA, anterior cerebral artery; brch., branch. Scale bars: 500µm

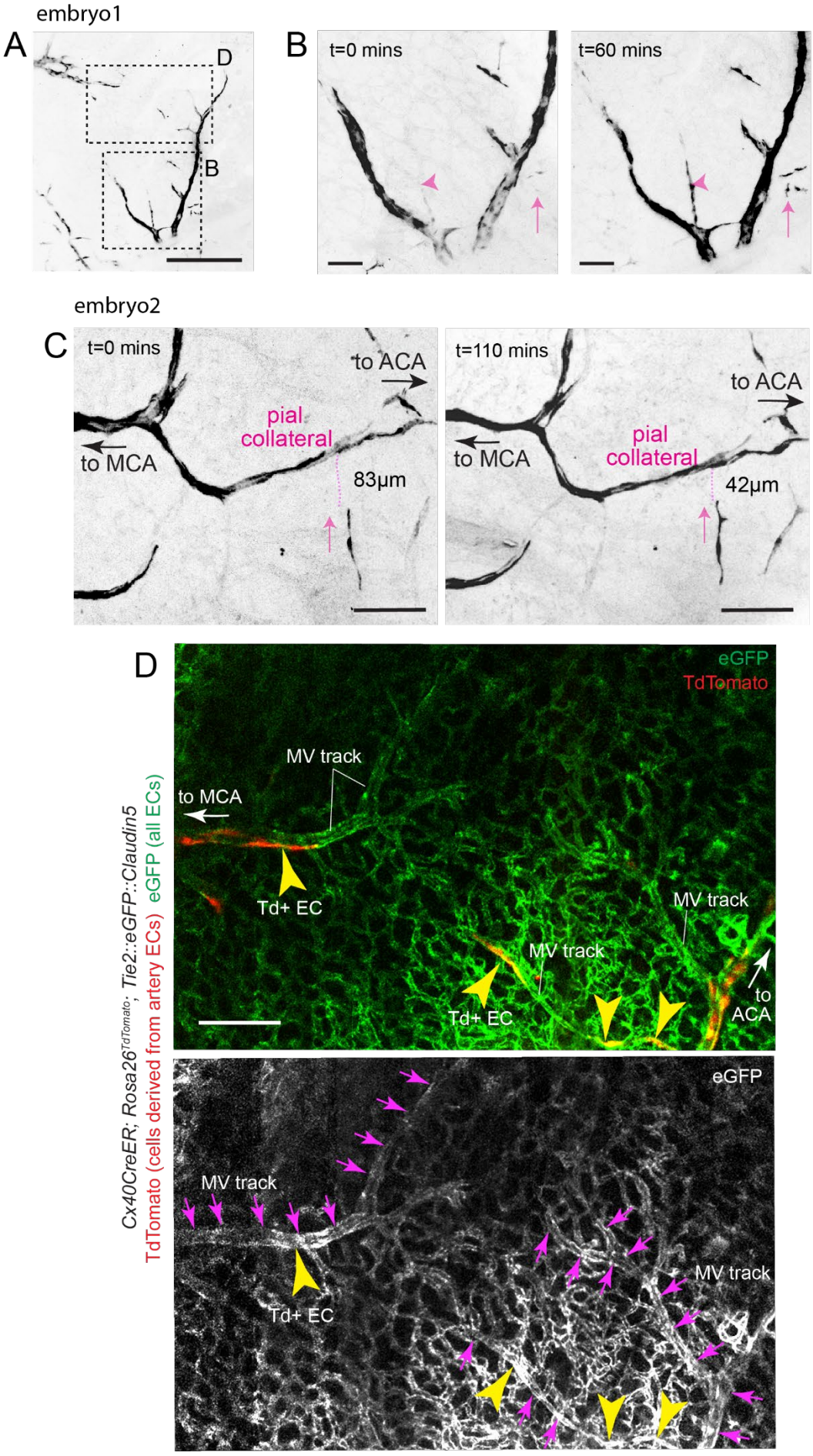
embryo1
A
D
B
B
t=0 mins
t=60 mins
embryo2
C
t=0 mins
to ACA
pial
collateral
to MCA
83µm
t=110 mins
to ACA
pial
collateral
to MCA
42µm
D
eGFP
TdTomato
MV track
to MCA
Td+ EC
MV track
MV track
Td+ EC
to
ACA
eGFP
MV track
Td+ EC
MV track
Cx40CreER; Rosa26TdTomato; Tie2::eGFP::Claudin5
TdTomato (cells derived from artery ECs) eGFP (all ECs)

944

945 **Supplemental Figure 4: Visualization of pial artery cell dynamics on**
946 **microvascular tracks** (**A**) Confocal image showing watershed region between MCA
947 and ACA of a live e16 embryo. (**B**) Inset from **A** showing growth of ACA in 60 mins.
948 Arrowhead point to an artery tip emerging at 60mins from imaging. Arrow points to
949 single artery cells. (**C**) Confocal image of e16 collateral zone showing single artery
950 endothelial cell migration towards the pial collateral in 110mins. Dotted line is the
951 length of micro-vessel between the single cell and the pial collateral. Magenta arrow
952 shows direction of single artery cell migration. (**D**) Inset from **A** showing presence of
953 TdTomato^{+} artery endothelial cells (yellow arrowheads) on eGFP^{+} microvascular
954 tracks (magenta arrows). MCA, Middle Cerebral Artery; ACA, Anterior Cerebral
955 Artery; MV, Microvascular; Td, TdTomato; EC, Endothelial cell. Scale bars: **A**,
956 500μm; **B**-**D**, 100μm.

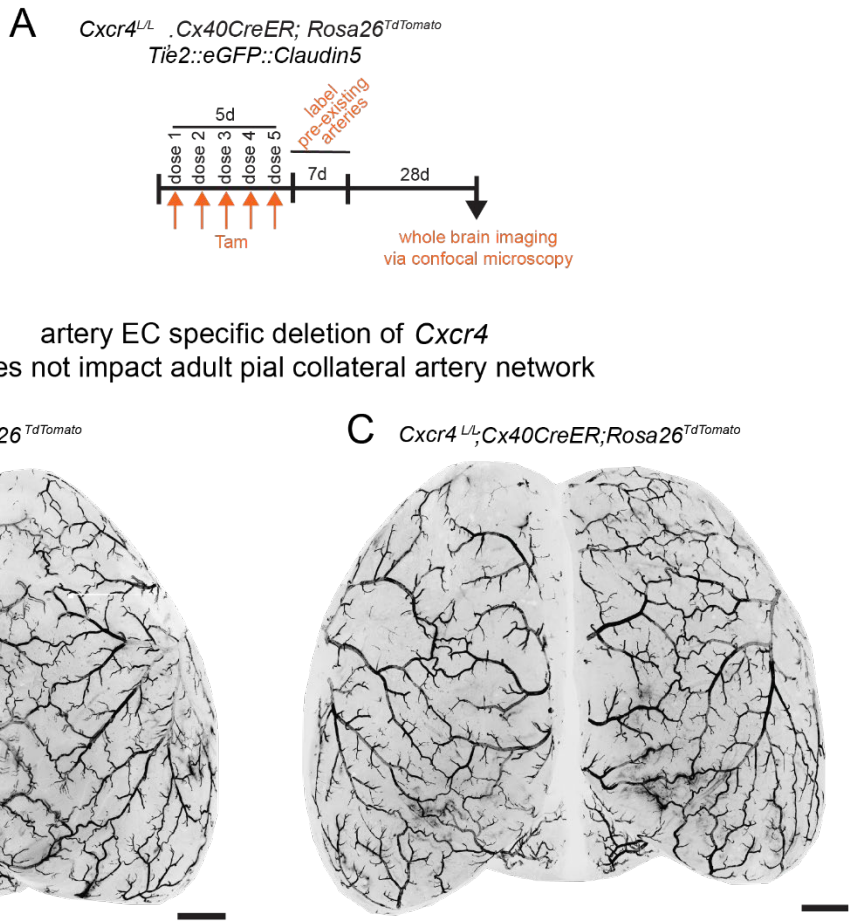

957

958

959

960

961

962

963

964

965

966 **Supplemental Figure 5: Pial artery coverage without arterial *Cxcr4*** (**A**)
967 Experimental set up to assess the effect of arterial *Cxcr4* deletion on pial artery
968 coverage in adults. (**B**, **C**) Confocal images of whole adult brains genetically lineage
969 traced for pre-existing artery endothelial cells, (**B**) with or (**C**) without arterial *Cxcr4*.
970 Scale bars: 1mm

971

972

973

974

975

976

977

978

979

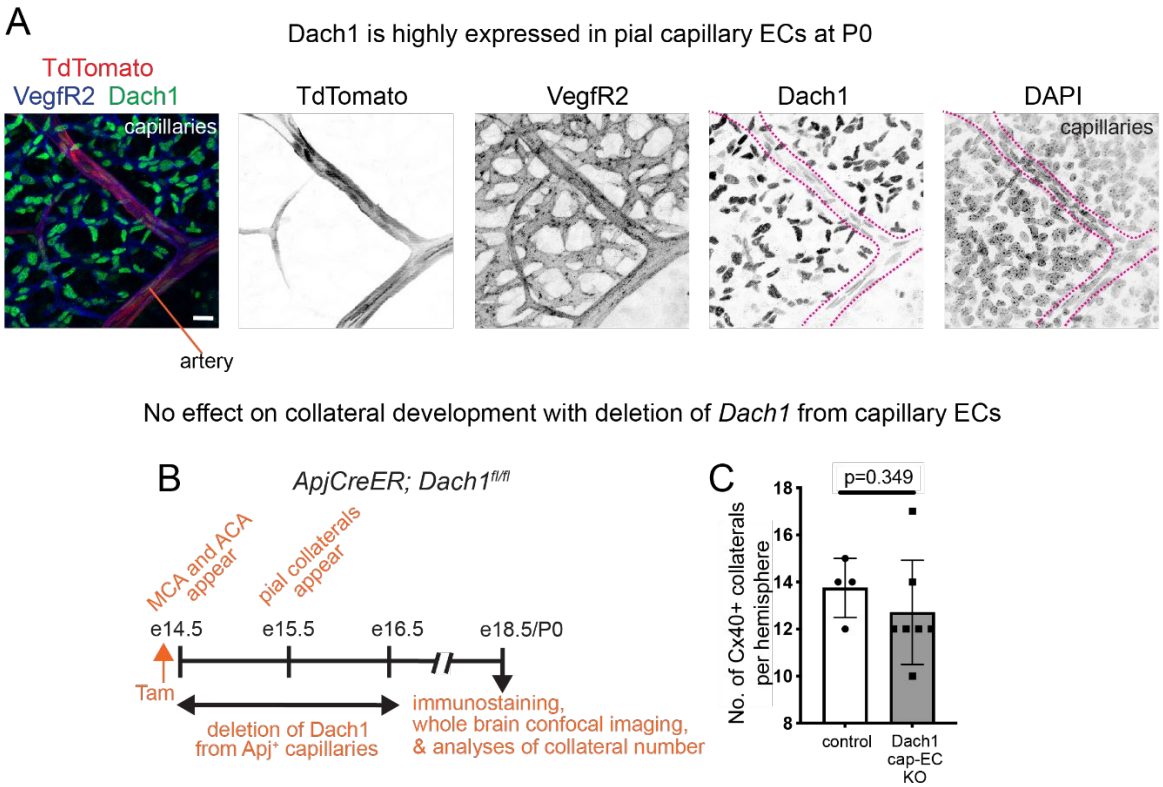

980

981

982

983

984

985

986

987

988

989

990

991 **Supplemental Figure 6: Dach1-independent pial collateral development** (**A**)
992 Dach1 expression in capillaries and arteries in P0 brains. (**B**) Experimental design
993 showing Tamoxifen injection at e14.5, and analyses of collateral numbers in e18.5
994 brains. Quantification of (**C**) Cx40^{+} pial collaterals between MCA and ACA in control
995 (*Dach1*$^{fl/fl}$) and *ApjCreER*; *Dach1*$^{fl/fl}$ (Dach1 cap-EC KO) brains. e, embryonic; SMA,
996 α-smooth muscle actin, cap-EC, capillary endothelial cell; KO, knockout. Scale bar:
997 20μm.

998

Intra-vital imaging of VefR2 deficient pial collaterals in adult mice

VegfR2$^{L/L}$ Cx40CreER; Rosa26^{TdTomato}
Tie2::eGFP::Claudin5
TdTomato (pre-existing artery ECs) eGFP (all ECs)

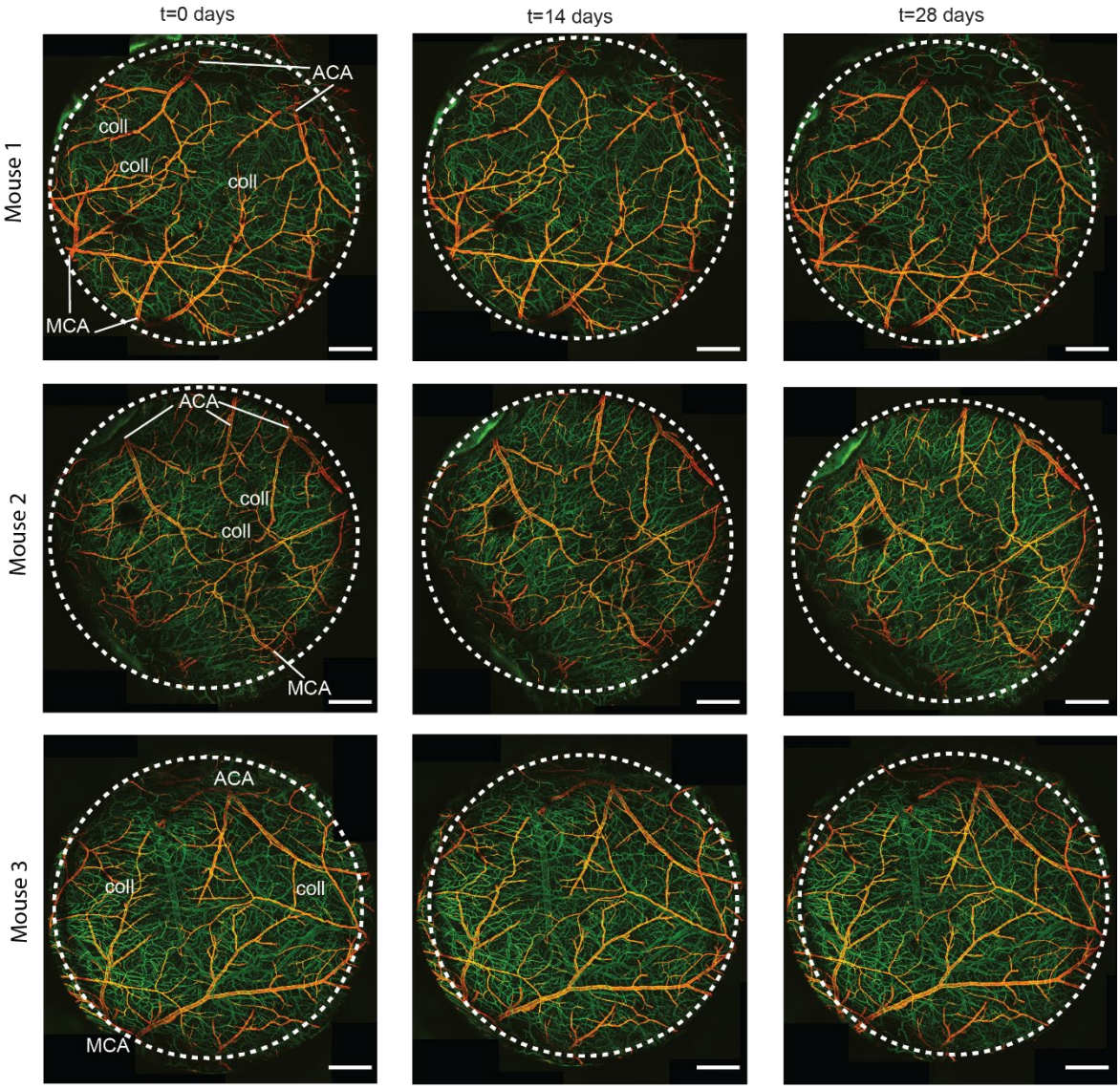

1005 **Supplemental Figure 7: VegfR2-independent maintenance of pial collaterals**

1006 Confocal images of the entire cranial window from 3 different mice shows that the
1007 overall pial artery network remains unchanged without arterial *VegfR2*. MCA, Middle
1008 Cerebral Arteries, ACA, Anterior Cerebral Arteries, Coll, Pial collateral arteries
1009 between MCA and ACA. Scale bars: 500μm.